Title: Rejuvenation of Senescent Cells by Low Frequency Ultrasound without Senolysis

Authors: Sanjay Kureel[1], Rosario Maroto[1], Simon Powell[1], Felix Margadant[2], Brandon Blair[1], Blake B. Rasmussen[1,3], Michael Sheetz[1*]

Affiliations:

[1]Biochemistry and Molecular Biology, University of Texas Medical Branch; 301 University Blvd., Galveston, Texas, 77555.
[2]Visiting Scientist, Biochemistry and Molecular Biology, University of Texas Medical Branch; 301 University Blvd., Galveston, Texas, 77555.
[3]Department of Biochemistry & Structural Biology, Sam and Ann Barshop Institute for Longevity and Aging Studies, University of Texas Health Sciences Center, San Antonio, TX, 78229.

*Corresponding author. misheetz@utmb.edu

Abstract:
It is believed that senescent cells are unable to grow; however, we have treated non-growing senescent cells with low frequency ultrasound (LFU) and they are rejuvenated for growth. Further, the senescent cells are characterized by low levels of motility but LFU treatment significantly increases the level of whole cell and organelle motility. At a mechanistic level, LFU causes Ca^{2+} entry that precedes dramatic increases in autophagy with the inhibition of mTORC1 and the movement of Sirtuin 1 from the nucleus to cytoplasm. Other characteristics of senescent cells are also reversed including blocking SASP secretion, restoring telomere length, plus nuclear 5mc levels, H3K9me3 levels, γH2AX levels, p53 nuclear staining, ROS and mitoROS levels are all restored to normal levels. Repeated LFU treatments enables expansion of primary cells and stem cells beyond normal replicative limits without altering cell phenotype. Rejuvenation is enhanced by rapamycin and Rho kinase inhibition but inhibited by blocking Sirtuin 1, Piezo1 or TRPV1. Thus, we suggest that mechanical pressure waves similar to those

generated by exercise can reverse senescence at the cell level, which provides a way to rejuvenate senescent cells in vivo.

One-Sentence Summary: Low frequency ultrasound alone rejuvenates senescent cells by activating autophagy.

Introduction:

Cell senescence is one of the hallmarks of the aging process that is characterized by a permanent block to cell growth (1-7). It was first noted in 1961, when Hayflick reported that primary cells in culture stopped growing after a certain number of divisions, i.e. they became senescent (*8*). Transplantation of senescent cells into young mice causes physical deterioration and age related pathologies (*9*), whereas depletion of these cells from aged mice slows age-related pathologies and enhances life span (*10-18*). This indicates that cellular senesence is one of the drivers of the aging process and removing senescent cells is critical for improving performance in aged organisms. Because senescence is believed to be a state of permanent cell cycle arrest where cells are metabolically active but stop dividing (*19*), the selective lysis of senescent cells is considered the best way to remove their negative effects (*20-23*). The alternative is to block the transition to the senescent state but that requires early intervention and is not applicable to aged individuals with senescent cells. Physical exercise is one early intervention to slow aging that is widely accepted (*24-26*) and has even been considered as a senolytic (*22*). Although the effects of exercise could be purely physical, there is evidence that exercise affects the brain and other organs through increased secretion of the myokines such as irisin (*27*). We report here that, surprisingly, physical pressure waves of low frequency ultrasound (LFU) can restore senescent cell growth by rejuvenating them.

Because the accumulation of senescent cells in tissues causes age-related pathologies (*28-30*), including in lung, adipose tissue, aorta, pancreas, and osteoarthritic joints (10), there are potentially many benefits from decreasing the fraction of senescent cells in tissues. The senescence process has general physiological significance since it prevents the propagation of damaged cells, suppresses tumor progression, helps in early development (*31*), wound healing (*32*), and in tissue repair processes (*33*). Despite the beneficial roles of senescent cells, there are many age-associated maladies (*34-36*). Senescent cells secrete many pro-inflammatory molecules, growth factors, chemokines, extracellular matrices, proteases and cytokines, collectively known as senescence associated secretary phenotype (SASP) (*37, 38*). An increase in the level of SASP catalyzes many age-related

problems (*39, 40*). Therefore, targeted elimination of senescent cells by senolytics can potentially improve age-associated pathologies including osteoarthritis (2), diabetes (*41*), osteoporosis, neurodegenerative disease (*42*), and overall lifespan (*10*). Senolytics have received considerable attention as a way to diminish specific effects of aging in tissues targeted by senolytics (*43*), (*13, 44, 45*) and have gone to clinical trials (*41*). However, there is currently no approved senolytic treatment for humans (*11, 46, 47*).

Autophagy inhibition and mitochondrial dysfunction are hallmarks of aging and cellular senescence (1). Dynamic changes in mitochondrial fusion and fission are essential for healthy mitochondrial function and increased fusion contributes to cell senescence (*19*). There is evidence of decreased senescence with exercise (*48*) that may be related to unknown processes that increase mitochondrial fission (*49, 50*). Although changes in lysosome and mitochondrial functions may be related, there is significant evidence that inhibition of lysosomal autophagy is a driver for aging (*51-53*).

Mutations in the genome can increase the lifespan of worms and flies and they are largely linked to metabolism and proteostasis pathways that inhibit the onset of senescence but do not reverse senescence at the cell level (*45, 46*). Strategies to prolong lifespan, including the use of small molecules (e.g. rapamycin) and caloric restriction, often can activate autophagy.

Ultrasound treatment can reverse cell senescence. We report here that ultrasound treatment can rejuvenate senescent cells without senolysis. Ultrasound produces short duration pressure waves in cells that create mechanical stresses. These conditions are safe for normal tissues and do not adversely influence functions of normal cells (*54*). In cases of chemically induced and replicative senescent cells that are blocked for growth, low frequency ultrasound (LFU) treatment can restore growth. LFU activates autophagy, organelle and cell motility, inhibits mTORC1, SASP secretion, β-galactosidase expression, decreases cell size, and mitochondrial length. Surprisingly, we find that normal cells treated with LFU secrete factors that activate senescent cell growth. Thus, purely mechanical stimuli can rejuvenate senescent cells.

RESULTS

Development and optimization of LFU

Since our previous studies showed that low frequency ultrasound (LFU) caused apoptosis of cancer cells *(31)*, we tested if LFU similarly caused apoptosis of senescent vero cells. To our surprise, the senescent cells grew instead. We then tested the effect of different ultrasound frequencies and power levels on the growth of the senescent cells and found that the stimulated growth was greater at 33 kHz than 39 kHz and peaked at a power level of 4 Pa as measured by a calibrated hydrophone (Figure S1C &D). The LFU bath had a peak power at the center and cells were positioned 7-10 cm above the ultrasound transducer to put them in the far field of the ultrasound (Figure S1A&B). We also optimized the effects of LFU duration of treatment and duty cycle (on/off times) on the growth rate of senescent cells (Figure S1E &F). Once we determined the optimum parameters; 32.2 kHz at 4 Pa for 30 mins with a duty cycle of 1.5s on and 1.5s off, we used those parameters for subsequent cell and mouse experiments.

To test the generality of LFU treatments for reversing cell senescence, we induced cell senescence with four compounds: doxorubicin, hydrogen peroxide, sodium butyrate and bleomycin sulfate by treating cells for 36-48 hours in the presence of the drug followed by 4 days of incubation in medium (*59*). Senescence was characterized by a block to growth (not different from zero growth statistically), increased β-galactosidase activity (>90% of cells were positive), increased cell size, and secretion of pro-inflammatory factors called SASP (*30*, *37*). All four criteria were met with each type of senescent cells (Fig. 1A) in that cell growth was blocked (Figure 1B), cell size increased (Figure 1C and 1D) (27), cells secreted SASP (15)

(Figure 1E) and β-galactosidase activity increased in over 98% of cells (Figure 1F and 1G). Thus, by all criteria, the cells were senescent.

Senescent Cells Are Rejuvenated for Growth

Drug-treated cells may have been quiescent and a fraction may have been partially senescent. Quiescent cells were characterized by the absence of β-galactosidase. The drug-treated cells were stained with β-galactosidase and over 95% of cells were stained after a four day incubation (*59*). Thus, there was not a significant fraction of quiescent cells in these preparations. To further test if the cells were senescent and if the senescent cells were reactivatable, we followed the cells by video microscopy for days. The Bleomycin sulfate treated cells were incubated for 22 days to assure that they were senescent before videotaping them for 24 hours (Figure 2A). There were no mitotic events (Figure 2B and F) and the cell migration was low as measured by the hourly displacements of the nuclei (Figure 2E). After LFU treatment for 30', however, over 30% of the cells divided in the next 48 hours (Figure 2C, D and F). Cell migration rate as measured by nuclear displacements increased by a factor of 2 from the senescent cells (Figure S2A). Thus, fully senescent cells were activated for growth and motility by LFU.

To determine if organelle motility was also activated, we followed the movements of the mitochondria. The mitochondria of senescent cells were often fused and were longer than usual (Figure 3 A). To determine the velocities of movement mitochondria positions of mitotracker labelled mitochondria were recorded every 1-2 minutes. After LFU treatment, the mitochondria were smaller (Figure 3C) and the linear velocities were dramatically increased by over 5 fold from before LFU treatment (Figure 3D). In addition, there were many mitochondrial fission and fusion events after LFU. For consistency, we only recorded the velocities of mitochondria that did not undergo fission or fusion during the observation period. Thus, the LFU treatment

activated both whole cell and mitochondrial movements, which meant that both actin and microtubule-based motility was increased after LFU.

LFU Rejuvenates Senescent Cells without senolysis

To determine if mechanical activity could reverse all types of the senescent cells, we treated different senescent cells (H2O2, bleomycin sulfate (BS), doxorubicin (Dox), sodium butyrate (SB), and replicative senescent cells) with LFU at the optimal power levels. After irradiation for thirty minutes, cells grew significantly (Figure S2 and S3). After the first passage, the growth rate of BS cells exceeded that of the parent line (Figure S2B). When LFU activation of the sodium butyrate, hydrogen peroxide and doxorubicin-treated senescent lines was measured, there was significant growth, but the growth rate was lower than BS (Fig. S2C). In the first two days, large cells divided, and the distribution of cell sizes shifted to smaller sizes, indicating that cells became smaller with growth, reaching normal cell size over 8-10 days (Figure S2C). When we analyzed the senescent cell populations after LFU treatment for apoptosis, there was none, indicating that LFU did not have a senolytic effect (Fig. S4). Cells grew after a single LFU treatment for 12-15 days without significantly decreasing in growth rate (Figure S2D). LFU treated cells had a reduced level of cell cycle inhibitor p21 (Figure S2E and S2F). Thus, by many criteria, LFU treatment activated growth of senescent cells without senolysis.

When senescent cells were stained for other senescence markers, there were dramatic decreases after LFU treatment. In particular, the senescence markers including p53 levels, γH2AX foci, H3K9me3 levels, cellular ROS and mitochondrial ROS levels were all decreased after LFU treatment in SB induced Vero cells (Figure 4). Thus, by many criteria, LFU treatment caused a dramatic decrease in the senescent state markers.

LFU Inhibits SASP Secretion

LFU treatment of SASP secreting senescent cells blocked further secretion of SASP as measured by the effects of pre- and post-LFU cell supernatants on normal cell growth (Fig. S5A-S5D). In a separate experiment where we measured the levels of SASP components in supernatants from senescent HFF cells before and after LFU treatment, the levels of eight SASP components decreased including Interleukines IL-6, IL-8, IL10, IL-15, and pro-inflammatory molecules TNF-α, IFN-γ, VEGF, MIP-1a (Fig. S5E). Thus, we suggest that LFU rejuvenates senescent cells including blocking the secretion of SASP components.

LFU of Normal Cells Causes Secretion of Components that Activate Senescent Cell Growth

Many studies have shown that physical exercise delays tissue and brain aging (*22*, *48*). To test the possibility that LFU could benefit senescent cells through an indirect effect on normal cells, we treated normal Vero cells with LFU over a period of three days (1 h per day) and then collected the ultrasound supernatant (USS) for culturing senescent Vero cells (Figure 5A). Surprisingly, USS activated growth of senescent cells (Figure 5B and 5C) and decreased their spread area (Figure 5D). We also assayed the levels of chemokines and cytokines in the supernatants from P3 HFFs after 3 days and in the USS (Figure 5E). The levels of IL-9, IL-17, MCP-1, MIP-1a, MIP-1b, RANTES, GM-CSF, EOTAXIN, G-CSF, and IP-10 components decreased whereas the levels of PDGF and VEGF increased (Figure 5E). Thus, LFU treatment of normal cells stimulated secretion of factors that caused growth of senescent cells.

LFU Activates Ca^{2+} entry, Autophagy and Inhibits mTORC1

If LFU was activating growth by activating autophagy downstream of Ca^{2+} entry as suggested in our working model (Figure 3D), then we should see Ca^{2+} loading and autophagy activation rapidly with LFU treatment. The time course of the Ca^{2+} entry was somewhat slow and it took 1-2 minutes before Ca^{2+} waves were evident (Figure 6A, B). Autophagy have been

activated by several processes (*55*) and it was not surprising that we saw significant changes in autophagy level (Figure 6C, D). Further, inhibition of autophagy by chloroquine diphosphate (CCD) blocked growth activation. Still, LFU activated autophagy even (Figure 6D) in presence or absence of the CCD inhibitor (lower GFP fluorescence intensity showed increased autophagy). Further, rapamycin was known to activate autophagy by inhibiting mTORC1, which was synergistic with LFU (*51*). L-Leucine (LL) activated mTORC1 and LL treated cells had higher levels of phosphorylated mTOR and rapamycin was antagonistic to mTOR phosphorylation. We observed that the level of phosphorylated mTOR was decreased by LFU (Figure S6). As expected, LFU activation of senescent cell growth was increased by rapamycin (Figure S7). Another protein linked to senescence was sirtuin1, an analog of the yeast deacetylase ser1 that inhibited senescence (*56*). When we inhibited sirtuin1 during LFU treatment of senescent cells, we found that rejuvenation of senescence was blocked (Figure S7). Thus, this indicated that NAD+-dependent deacetylation was needed for rejuvenation of senescent cells by LFU. Other factors have been linked to aging and cell senescence, including telomere shortening (*44*) and DNA hypomethylation (*43*). In the case of telomere length, there was a significant increase in the average telomere length of replicatively senescent fibroblasts after LFU treatment (Figure S8B) and a smaller increase in mesenchymal stem cells (Figure S8C). DNA methylation levels of senescent cells were increased by LFU, which was consistent with the rejuvenation of senescent cells by LFU (Figure S8) and with the decrease in H3K9me3 levels after LFU (Fig. 4). Thus, LFU treatment of senescent cells reverses senescence-dependent changes in the nucleus, consistent with a restoration of the normal cell state by LFU.

Plasma membrane ion Channels are Needed for Rejuvenation

The first organelle of a cell that encounters LFU is the plasma membrane. Piezo1 ion channels are activated by the LFU and play a major role in tumor cell apoptosis (*55*). We

checked the expression level of piezo1 and other ion channels including TRPV1 and measured if their activation by LFU was important for the process of rejuvenation. Incubation of SCs with the Piezo1 inhibitor, GsMTx4, inhibited cell growth after LFU treatment (Figure S9. Further, when SCs were treated with LFU in presence of Ruthenium Red, an inhibitor of TRPV1, we also observed decreased growth of senescent cells after 48 h (Figure S9). Thus, we suggest that LFU stimulation of growth depended upon the mechanical ion channels piezo1 and TRPV1.

RNAseq analysis of the changes in mRNA levels of senescent cells upon LFU rejuvenation revealed that the expression levels of 50 genes were upregulated by a factor of two or more upon rejuvenation whereas 140 genes were downregulated (Table 1 and 2). Of particular interest were the SASP proteins that were downregulated upon rejuvenation, which included IGF2, IGFBP2, FGF7 and C1Q-TNF7. Further pathway analysis was done which indicated that many of the genes activated by LFU were in pathways activated by viral infections (Table 3 and 4) This was consistent with the activation of the cells and reversal of the senescent state upon rejuvenation.

Previous studies from our laboratory reported that a different ultrasound treatment caused apoptosis of tumor cells but not normal cells (*57*). In that case, LFU-dependent tumor cell apoptosis increased after microtubule depolymerization by nocodazole and the Rho kinase inhibitor (Y-27632) blocked apoptosis. Depolymerization of microtubules increased Rho kinase activity and myosin contractility (*58*) whereas the Rho kinase inhibitor decreased contractility. In the case of LFU induced senescent cell rejuvenation, addition of Y-27632 increased rejuvenation while microtubule depolymerization by nocodazole had no effect (Figure S7E). Thus, the reversal of senescence by LFU was different from the activation of tumor cell apoptosis, since it involved different cytoskeletal elements.

Expansion of Replicative Senescent Cells by LFU

Because replicative senescence presumably was a common property of normal cells that limited growth (*8*), we tested whether LFU could extend the growth potential of normal cells. After 15 passages human foreskin fibroblasts (HFFs) decreased in growth rate, increased in average cell size, and exhibited increased β-galactosidase activity. However, after LFU treatment with every other passage, for passages 15-24, HFF cells behaved like normal cells and continued to grow without a significant change in growth rate for at least 24 passages (Figure 7A). This made it possible to grow >7,500 (2^{13}) fold more HFF cells than without LFU, while spread area was normal (Figure 7B) and there was no increase in senescence markers (Figure 4C). When P24 LFU cells were cultured on soft matrices, they ceased to grow, showing rigidity-dependent growth. Similarly, we expanded mesenchymal stem cells (MSCs) with LFU beyond the normal replicative limit (Figure 7D). Upon treatment with differentiation medium, the LFU expanded MSCs differentiated into adipocytes or osteocytes, depending upon the medium (Figure 7E, F & G) although the level of adipocyte differentiation was higher in the LFU treated cells than in the replicatively senescent MSCs.

Discussion

These studies show that rigorously senescent cells can be mechanically rejuvenated by LFU without transfection or other biochemical manipulations. The ultrasound pressure waves restore normal behavior irrespective of whether senescence is induced by chemical treatment or by repeated replication. There is no apoptosis with LFU and videos of senescent cells before and after LFU show a dramatic increase in cell motility as well as growth after whereas there was no growth before LFU. Features of senescent cells are all reversed by LFU, including the increase in β-galactosidase activity, p21 expression, decreased telomere length, increased H3K9me3 levels, decreased 5mc levels, increased cell size, secretion of SASP and inhibition of growth. Restoration of normal behavior correlates with a decrease in mitochondrial length and lysosomal

volume. There are optimal values of LFU power, frequency and duty cycle for rejuvenation of senescent cells that belie an unknown set of processes that are mechanically activated by LFU. Surprisingly, ultrasound treatment of normal cells causes secretion of growth stimulating factors that partially restore normal behavior in senescent cells. Because replicative senescent cells are restored to a normal phenotype by LFU, they can be cultured for long periods to produce increased numbers of cells without major alteration in phenotype.

It is perhaps surprising to many that fully senescent cells are rejuvenated by pressure waves. This raises the question of how a senescent cell is defined. We were careful to incubate cells that were made senescent by toxic compounds or repeated replications for long periods and time lapse video microscopy verified the absence of any growth. We can rule out the possibility that we activated quiescent cells since over 95% of the cells expressed β-galactosidase after incubation (*59*) and many of the larger senescent cells grew and divided in the videos. By tracing individual cells, it was possible to determine that growth was occurring in over 50% of the originally non-dividing cells after 4-5 days. Such robust growth is inconsistent with the growth occurring in a subpopulation of cells that were not senescent. Further, there was no apoptosis after LFU treatment of our senescent cells. Thus, because of all of these objective criteria for the reversal of senescence, we suggest that senescent cells can be rejuvenated by LFU. This opens many new possibilities in aging research including rejuvenating aged cells in vivo to inhibit age-dependent disorders.

The selective lysis of senescent cells is an alternative approach to reducing the effects of aging, and it has been shown to improve performance of older mice (*13, 43, 60, 61*) 37). The obvious difficulty is that the loss of senescent cells is hard to reverse and the stimulation of growth of the remaining non-senescent cells will stress them and encourage their senescence. In separate studies, we have found that LFU treatment will improve the physical performance of

aged mice (*62*). Thus, it seems from preliminary studies that LFU can be used to rejuvenate aged animals without the use of senolytics.

Mechanical effects on cell behavior have been known for a long time. However, recently it has become clear that controlled mechanical perturbations can reproducibly alter cell functions and phenotypic behaviors. Tumor cells are mechanosensitive since either stretching, fluid shear or ultrasound can cause apoptosis in vitro (*57, 63, 64*). In addition, exercise appears to inhibit tumor growth in vivo (*65*). Normal cells appear to do better with exercise and myokines that are released with exercise benefit the organism. In the studies presented here, LFU stimulation of normal cells causes the release of beneficial factors that stimulate growth of senescent cells and perhaps could augment the LFU rejuvenation of aged cells in tissues.

There is evidence of a correlation between exercise and a reversal of senescent cells in older animals and humans (*48*). Individual cells have not been followed and it is not clear if exercise reverses senescence or is a Senolytic (28). In these studies, it is clear that ultrasound pressure waves alone can reverse senescent cell to normal cell behavior, i.e. rejuvenate them, without causing cell death in vitro. The ultrasound and exercise effects in vivo are synergistic and both will cause cell deformations. We suggest that both exercise and LFU will rejuvenate cells in situ without apoptosis and thereby increase the performance of aged animals. Because LFU can easily penetrate the whole human body with only significant loss of power in bone and lung, it can rejuvenate most of the tissues including internal organs like pancreas and kidney that will not be particularly sensitive to exercise. A critical issue for improving the performance of aged animals is that the level of SASP and other inhibitory factors in the animal decreases, through either senolytics, exercise or LFU.

The senescent cell state has been extensively studied but the molecular bases for the changes are not fully understood. It is noteworthy that Ca^{2+} transients occur soon after LFU

stimulation and Ca^{2+} is needed for activation of autophagy (*62*). In addition to autophagy, there are major roles for changes in mitophagy in senescence (*51, 56, 66-69*). Accordingly, most models of the senescence process postulate complicated roles for autophagy and mitophagy to couple changes in activity of lysosomes, mitochondria and other cellular organelles with the cell cycle (*48, 49*). The subcellular effects of ultrasound appear to be mediated by Ca^{2+} effects on mechanically dependent mitochondria-ER-lysosome interactions, which activate lysosomal autophagy and mitochondrial fission that is a requisite for mitophagy. Thus, we suggest that LFU induced distortion acts on organized elements of the cytoplasm like exercise to reverse complexes induced by aging. Similarly, the increase in motile activity caused by LFU indicates that there is a general effect on cells to restore normal functions that are slowed in senescent cells by the accumulation of damaged material. At a molecular level, senescence is associated with active mTORC1 binding to lysosomes thereby inactivating autophagy (*70, 71*). Rapamycin inhibition of mTORC1 is synergistic with LFU-induced rejuvenation and rejuvenation involves activation of autophagy (Figure S6) and a decrease in lysosomal staining (Figure 3B). In the case of Sirtuin 1, loss of activity is associated with an increase in senescence, which fits with the need for Sirtuin 1 activity in rejuvenation (Figure S7) (*56*). In addition, AMPK plays a major role in mitophagy and autophagy and its activation by AICAR increases the performance of aged mice (*50*). Piezo1 and/or TRPV1 ion channel activity is needed for optimal LFU rejuvenation of senescent cells and appears to have a role in endothelial cell aging (*54*). The ruthenium red inhibitor may have off-target effects and selective inhibitors are needed to understand how the relatively slow Ca^{2+} waves might be involved in rejuvenation. In general, much more research is needed to understand how LFU pressure waves could activate autophagy, inhibit mTORC1 and activate Sirtuin1 enzyme function to stimulate cell growth.

Cellular changes with senescence are extensive and involve not only changes in organelle architecture but also in the secretory pathways that produce SASP. The surprising finding of growth stimulatory factors that are secreted by normal cells upon LFU stimulation indicates that LFU mechanical effects may be part of a larger network of functions that support systemic responses to physical exercise. For example, exercise stimulates the secretion of myokines that benefit brain function and quality of life (*72*). We suggest that the effects of LFU mimic many of the effects of exercise at a cellular level with the added benefit that LFU can penetrate the human body to reach internal organs.

The activation of growth of replicative senescent cells by non-invasive LFU has important implications for the in vitro expansion of normal cells to aid in autologous repair procedures and it can augment the effects of nicotinamide on replicative senescence (*73*). Much more research is needed to understand the extent of the expansion that is possible. However, we find that expansion does not involve apparent damage to the cells or major modifications of their phenotype. This indicates that the ultrasound reversal of senescence can have significant benefits in enabling the continued growth of normal cells beyond current limits.

Since ultrasound has been approved for human exposure at power levels ten to hundred-fold higher than the optimal levels used in this study, we suggest that it is practical to develop ultrasound-based therapies that could inhibit the increase in senescent cells in tissues with aging and thereby inhibit the onset of many age-related maladies. This non-invasive procedure has advantages over senolytics and exercise in that it is not tissue selective. In addition, LFU is non-invasive and will not directly affect biochemical or molecular biological treatments. Most importantly, these results show that mechanical treatments can augment or replace biochemical treatments to produce desired reversal of senescence and they are consistent with known effects of exercise on senescence and quality of life with aging.

Acknowledgments:

We want to acknowledge the experimental help of Adam Baker. We greatly appreciated the advice in editing this manuscript provided by Linda Kenney. Dr. Felix Margadant and Simon Powell provided support in fabrication of ultrasound devices and their maintenance.

Funding:

UTMB Biochemistry and Molecular Biology Department startup funds (MS)

CPRIT Foundation grant RR180025 (MS)

Welch Foundation professorship (MS)

Claude D. Pepper Older Americans Independence Center Pilot Project Grant (MS and BR)

NSF grant 1933321 (Co-I MS)

Author contributions:

Conceptualization: MS, SK, BR

Methodology: SK, RM, SP, FM

Writing: MS, SK, BR,

Experimentation: SK, RM, BB

Competing interests: Authors (MS, SK, FM, and RM) are co-authors of patents related to these studies and MS and FM have financial interests in a company, Mechanobiologics, Inc that is planning to market LFU devices suitable for senescent cell rejuvenation.

Data and materials availability: All data are available in the main text or the supplementary materials.

REFEREMCES

1. M. Y. Terzi, M. Izmirli, B. Gogebakan, The cell fate: senescence or quiescence. *Mol Biol Rep* **43**, 1213-1220 (2016).
2. M. V. Blagosklonny, Cell senescence, rapamycin and hyperfunction theory of aging. *Cell Cycle* **21**, 1456-1467 (2022).

3. S. N. Mowla, N. D. Perkins, P. S. Jat, Friend or foe: emerging role of nuclear factor kappa-light-chain-enhancer of activated B cells in cell senescence. *Onco Targets Ther* **6**, 1221-1229 (2013).
4. J. P. de Magalhaes, J. F. Passos, Stress, cell senescence and organismal ageing. *Mech Ageing Dev* **170**, 2-9 (2018).
5. S. Victorelli, J. F. Passos, Telomeres and Cell Senescence - Size Matters Not. *EBioMedicine* **21**, 14-20 (2017).
6. H. Chandler, G. Peters, Stressing the cell cycle in senescence and aging. *Curr Opin Cell Biol* **25**, 765-771 (2013).
7. A. P. Beltrami, D. Cesselli, C. A. Beltrami, Stem cell senescence and regenerative paradigms. *Clin Pharmacol Ther* **91**, 21-29 (2012).
8. L. Hayflick, P. S. Moorhead, The serial cultivation of human diploid cell strains. *Exp Cell Res* **25**, 585-621 (1961).
9. M. Xu *et al.*, Transplanted Senescent Cells Induce an Osteoarthritis-Like Condition in Mice. *J Gerontol A Biol Sci Med Sci* **72**, 780-785 (2017).
10. M. Xu *et al.*, Senolytics improve physical function and increase lifespan in old age. *Nat Med* **24**, 1246-1256 (2018).
11. Y. Cai *et al.*, Elimination of senescent cells by beta-galactosidase-targeted prodrug attenuates inflammation and restores physical function in aged mice. *Cell Res* **30**, 574-589 (2020).
12. O. H. Jeon *et al.*, Local clearance of senescent cells attenuates the development of post-traumatic osteoarthritis and creates a pro-regenerative environment. *Nat Med* **23**, 775-781 (2017).
13. J. Chang *et al.*, Clearance of senescent cells by ABT263 rejuvenates aged hematopoietic stem cells in mice. *Nat Med* **22**, 78-83 (2016).
14. W. Peilin *et al.*, Directed elimination of senescent cells attenuates development of osteoarthritis by inhibition of c-IAP and XIAP. *Biochim Biophys Acta Mol Basis Dis* **1865**, 2618-2632 (2019).
15. T. J. Bussian *et al.*, Clearance of senescent glial cells prevents tau-dependent pathology and cognitive decline. *Nature* **562**, 578-582 (2018).
16. P. Patil *et al.*, Systemic clearance of p16(INK4a) -positive senescent cells mitigates age-associated intervertebral disc degeneration. *Aging Cell* **18**, e12927 (2019).
17. L. Caland *et al.*, Knockdown of angiopoietin-like 2 induces clearance of vascular endothelial senescent cells by apoptosis, promotes endothelial repair and slows atherogenesis in mice. *Aging (Albany NY)* **11**, 3832-3850 (2019).
18. J. B. Chae *et al.*, Targeting senescent retinal pigment epithelial cells facilitates retinal regeneration in mouse models of age-related macular degeneration. *Geroscience*, (2021).
19. B. G. Childs, M. Durik, D. J. Baker, J. M. van Deursen, Cellular senescence in aging and age-related disease: from mechanisms to therapy. *Nat Med* **21**, 1424-1435 (2015).
20. E. C. Lorenzo, B. L. Torrance, L. Haynes, Impact of senolytic treatment on immunity, aging, and disease. *Front Aging* **4**, 1161799 (2023).
21. K. Yamaura *et al.*, Therapeutic potential of senolytic agent quercetin in osteoarthritis: A systematic review and meta-analysis of preclinical studies. *Ageing Res Rev* **90**, 101989 (2023).
22. X. K. Chen *et al.*, Is exercise a senolytic medicine? A systematic review. *Aging Cell* **20**, e13294 (2021).
23. J. L. Kirkland, T. Tchkonia, Senolytic drugs: from discovery to translation. *J Intern Med* **288**, 518-536 (2020).

24. S. Chubanava, J. T. Treebak, Regular exercise effectively protects against the aging-associated decline in skeletal muscle NAD content. *Exp Gerontol* **173**, 112109 (2023).
25. A. De Sousa Lages *et al.*, Therapeutics That Can Potentially Replicate or Augment the Anti-Aging Effects of Physical Exercise. *Int J Mol Sci* **23**, (2022).
26. F. Galkin, O. Kovalchuk, D. Koldasbayeva, A. Zhavoronkov, E. Bischof, Stress, diet, exercise: Common environmental factors and their impact on epigenetic age. *Ageing Res Rev* **88**, 101956 (2023).
27. K. Ning, Z. Wang, X. A. Zhang, Exercise-induced modulation of myokine irisin in bone and cartilage tissue-Positive effects on osteoarthritis: A narrative review. *Front Aging Neurosci* **14**, 934406 (2022).
28. S. He, N. E. Sharpless, Senescence in Health and Disease. *Cell* **169**, 1000-1011 (2017).
29. P. D. Adams, Healing and hurting: molecular mechanisms, functions, and pathologies of cellular senescence. *Mol Cell* **36**, 2-14 (2009).
30. N. Herranz, J. Gil, Mechanisms and functions of cellular senescence. *J Clin Invest* **128**, 1238-1246 (2018).
31. M. Storer *et al.*, Senescence is a developmental mechanism that contributes to embryonic growth and patterning. *Cell* **155**, 1119-1130 (2013).
32. M. Demaria *et al.*, An essential role for senescent cells in optimal wound healing through secretion of PDGF-AA. *Dev Cell* **31**, 722-733 (2014).
33. D. Munoz-Espin, M. Serrano, Cellular senescence: from physiology to pathology. *Nat Rev Mol Cell Biol* **15**, 482-496 (2014).
34. B. G. Childs *et al.*, Senescent cells: an emerging target for diseases of ageing. *Nat Rev Drug Discov* **16**, 718-735 (2017).
35. D. McHugh, J. Gil, Senescence and aging: Causes, consequences, and therapeutic avenues. *J Cell Biol* **217**, 65-77 (2018).
36. M. Borghesan, W. M. H. Hoogaars, M. Varela-Eirin, N. Talma, M. Demaria, A Senescence-Centric View of Aging: Implications for Longevity and Disease. *Trends Cell Biol* **30**, 777-791 (2020).
37. A. R. Young, M. Narita, SASP reflects senescence. *EMBO Rep* **10**, 228-230 (2009).
38. T. Tchkonia, Y. Zhu, J. van Deursen, J. Campisi, J. L. Kirkland, Cellular senescence and the senescent secretory phenotype: therapeutic opportunities. *J Clin Invest* **123**, 966-972 (2013).
39. J. P. Coppe *et al.*, Senescence-associated secretory phenotypes reveal cell-nonautonomous functions of oncogenic RAS and the p53 tumor suppressor. *PLoS Biol* **6**, 2853-2868 (2008).
40. P. F. L. da Silva *et al.*, The bystander effect contributes to the accumulation of senescent cells in vivo. *Aging Cell* **18**, e12848 (2019).
41. P. J. Thompson *et al.*, Targeted Elimination of Senescent Beta Cells Prevents Type 1 Diabetes. *Cell Metab* **29**, 1045-1060 e1010 (2019).
42. J. Penney, L. H. Tsai, Elimination of senescent cells prevents neurodegeneration in mice. *Nature* **562**, 503-504 (2018).
43. Y. Zhu *et al.*, The Achilles' heel of senescent cells: from transcriptome to senolytic drugs. *Aging Cell* **14**, 644-658 (2015).
44. M. J. Yousefzadeh *et al.*, Fisetin is a senotherapeutic that extends health and lifespan. *EBioMedicine* **36**, 18-28 (2018).
45. Y. Zhu *et al.*, Identification of a novel senolytic agent, navitoclax, targeting the Bcl-2 family of anti-apoptotic factors. *Aging Cell* **15**, 428-435 (2016).

46. G. Libertini, N. Ferrara, G. Rengo, G. Corbi, Elimination of Senescent Cells: Prospects According to the Subtelomere-Telomere Theory. *Biochemistry (Mosc)* **83**, 1477-1488 (2018).
47. J. Neves, P. Sousa-Victor, H. Jasper, Rejuvenating Strategies for Stem Cell-Based Therapies in Aging. *Cell Stem Cell* **20**, 161-175 (2017).
48. D. A. Englund *et al.*, Exercise reduces circulating biomarkers of cellular senescence in humans. *Aging Cell* **20**, (2021).
49. E. Bartolak-Suki, J. Imsirovic, Y. Nishibori, R. Krishnan, B. Suki, Regulation of Mitochondrial Structure and Dynamics by the Cytoskeleton and Mechanical Factors. *Int J Mol Sci* **18**, (2017).
50. S. C. J. Helle *et al.*, Mechanical force induces mitochondrial fission. *Elife* **6**, (2017).
51. J. M. Carosi, C. Fourrier, J. Bensalem, T. J. Sargeant, The mTOR-lysosome axis at the centre of ageing. *FEBS Open Bio* **12**, 739-757 (2022).
52. L. D. Cassidy, M. Narita, Dynamic modulation of autophagy: implications for aging and cancer. *Mol Cell Oncol* **7**, 1754723 (2020).
53. D. C. Rubinsztein, G. Marino, G. Kroemer, Autophagy and aging. *Cell* **146**, 682-695 (2011).
54. F. Ahmadi, I. V. McLoughlin, S. Chauhan, G. ter-Haar, Bio-effects and safety of low-intensity, low-frequency ultrasonic exposure. *Prog Biophys Mol Biol* **108**, 119-138 (2012).
55. M. D. Bootman, T. Chehab, G. Bultynck, J. B. Parys, K. Rietdorf, The regulation of autophagy by calcium signals: Do we have a consensus? *Cell Calcium* **70**, 32-46 (2018).
56. T. Liu *et al.*, SIRT1 reverses senescence via enhancing autophagy and attenuates oxidative stress-induced apoptosis through promoting p53 degradation. *Int J Biol Macromol* **117**, 225-234 (2018).
57. A. Singh *et al.*, Enhanced tumor cell killing by ultrasound after microtubule depolymerization. *Bioeng Transl Med* **6**, e10233 (2021).
58. K. Chitaley, R. C. Webb, Microtubule depolymerization facilitates contraction of vascular smooth muscle via increased activation of RhoA/Rho-kinase. *Med Hypotheses* **56**, 381-385 (2001).
59. N. Alessio *et al.*, Different Stages of Quiescence, Senescence, and Cell Stress Identified by Molecular Algorithm Based on the Expression of Ki67, RPS6, and Beta-Galactosidase Activity. *Int J Mol Sci* **22**, (2021).
60. J. N. Farr *et al.*, Targeting cellular senescence prevents age-related bone loss in mice. *Nat Med* **23**, 1072-1079 (2017).
61. A. R. Mendelsohn, J. W. Larrick, Prevention of Senescence in Vasculature Through Quiescence. *Rejuvenation Res* **21**, 477-481 (2018).
62. S. Kumar *et al.*, Rejuvenating Senescent Cells and Organisms with Only Ultrasound. *bioRxiv*, 2022.2012.2008.519320 (2024).
63. M. Sheetz, A Tale of Two States: Normal and Transformed, With and Without Rigidity Sensing. *Annu Rev Cell Dev Biol* **35**, 169-190 (2019).
64. A. Tijore *et al.*, Selective killing of transformed cells by mechanical stretch. *Biomaterials* **275**, 120866 (2021).
65. H. Rundqvist *et al.*, Cytotoxic T-cells mediate exercise-induced reductions in tumor growth. *Elife* **9**, (2020).
66. J. H. Cho *et al.*, Downregulation of SIRT1 signaling underlies hepatic autophagy impairment in glycogen storage disease type Ia. *PLoS Genet* **13**, e1006819 (2017).

67. K. A. Escobar, N. H. Cole, C. M. Mermier, T. A. VanDusseldorp, Autophagy and aging: Maintaining the proteome through exercise and caloric restriction. *Aging Cell* **18**, e12876 (2019).
68. S. Kaushik *et al.*, Autophagy and the hallmarks of aging. *Ageing Res Rev* **72**, 101468 (2021).
69. Y. Xu, W. Wan, Acetylation in the regulation of autophagy. *Autophagy*, 1-9 (2022).
70. A. Bartolome *et al.*, MTORC1 Regulates both General Autophagy and Mitophagy Induction after Oxidative Phosphorylation Uncoupling. *Mol Cell Biol* **37**, (2017).
71. Z. Zi *et al.*, Quantitative phosphoproteomic analyses identify STK11IP as a lysosome-specific substrate of mTORC1 that regulates lysosomal acidification. *Nat Commun* **13**, 1760 (2022).
72. B. So, H. J. Kim, J. Kim, W. Song, Exercise-induced myokines in health and metabolic diseases. *Integr Med Res* **3**, 172-179 (2014).
73. C. S. Lim, M. Potts, R. F. Helm, Nicotinamide extends the replicative life span of primary human cells. *Mech Ageing Dev* **127**, 511-514 (2006).
41. J. L. Kirkland, T. Tchkonia, Y. Zhu, L. J. Niedernhofer, P. D. Robbins, The Clinical Potential of Senolytic Drugs. *J Am Geriatr Soc* **65**, 2297-2301 (2017).
42. Bu L, Luo T, Yan J, Li G, Huang J. Single-molecule analysis of genome-wide DNA methylation by fiber FISH coupled with atomic force microscopy. Analyst. 2022;147(8):1559-66
43. D. Gentilini *et al.*, Role of epigenetics in human aging and longevity: genome-wide DNA methylation profile in centenarians and centenarians' offspring. *Age (Dordr)* **35**, 1961-1973 (2013).
44. R. Farahzadi, E. Fathi, S. A. Mesbah-Namin, N. Zarghami, Zinc sulfate contributes to promote telomere length extension via increasing telomerase gene expression, telomerase activity and change in the TERT gene promoter CpG island methylation status of human adipose-derived mesenchymal stem cells. *PLoS One* **12**, e0188052 (2017).
45. W. H. Zhang, S. Koyuncu, D. Vilchez, Insights Into the Links Between Proteostasis and Aging From C. elegans. *Front Aging* **3**, 854157 (2022).
46. H. Lee, S. V. Lee, Recent Progress in Regulation of Aging by Insulin/IGF-1 Signaling in Caenorhabditis elegans. *Mol Cells* **45**, 763-770 (2022).
47. Z. Yang *et al.*, Multi-Omics Comparison of the Spontaneous Diabetes Mellitus and Diet-Induced Prediabetic Macaque Models. *Front Pharmacol* **12**, 784231 (2021).
48. J. Huang, P. Meng, C. Wang, Y. Zhang, L. Zhou, The relevance of organelle interactions in cellular senescence. *Theranostics* **12**, 2445-2464 (2022).
49. O. Moltedo, P. Remondelli, G. Amodio, The Mitochondria-Endoplasmic Reticulum Contacts and Their Critical Role in Aging and Age-Associated Diseases. *Front Cell Dev Biol* **7**, 172 (2019).
50. T. Kobilo *et al.*, AMPK agonist AICAR improves cognition and motor coordination in young and aged mice. *Learn Mem* **21**, 119-126 (2014).
51. A. Dobin *et al.*, STAR: ultrafast universal RNA-seq aligner. *Bioinformatics* **29**, 15-21 (2013).
52. A. Frankish *et al.*, GENCODE reference annotation for the human and mouse genomes. *Nucleic Acids Res* **47**, D766-D773 (2019).
53. A. Dobin *et al.*, STAR: ultrafast universal RNA-seq aligner. *Bioinformatics* **29**, 15-21 (2013).
54. Xiao, T., et al. "TRPV1: A promising therapeutic target for skin aging and inflammatory skin diseases." Front Pharmacol **14**: 1037925 (2023).

55. M. Yao *et al.*, Force- and cell state-dependent recruitment of Piezo1 drives focal adhesion dynamics and calcium entry. *Sci Adv* **8**, eabo1461 (2022).

56. A. Hernandez-Segura, J. Nehme, M. Demaria, Hallmarks of Cellular Senescence. *Trends Cell Biol* **28**, 436-453 (2018).

Figures

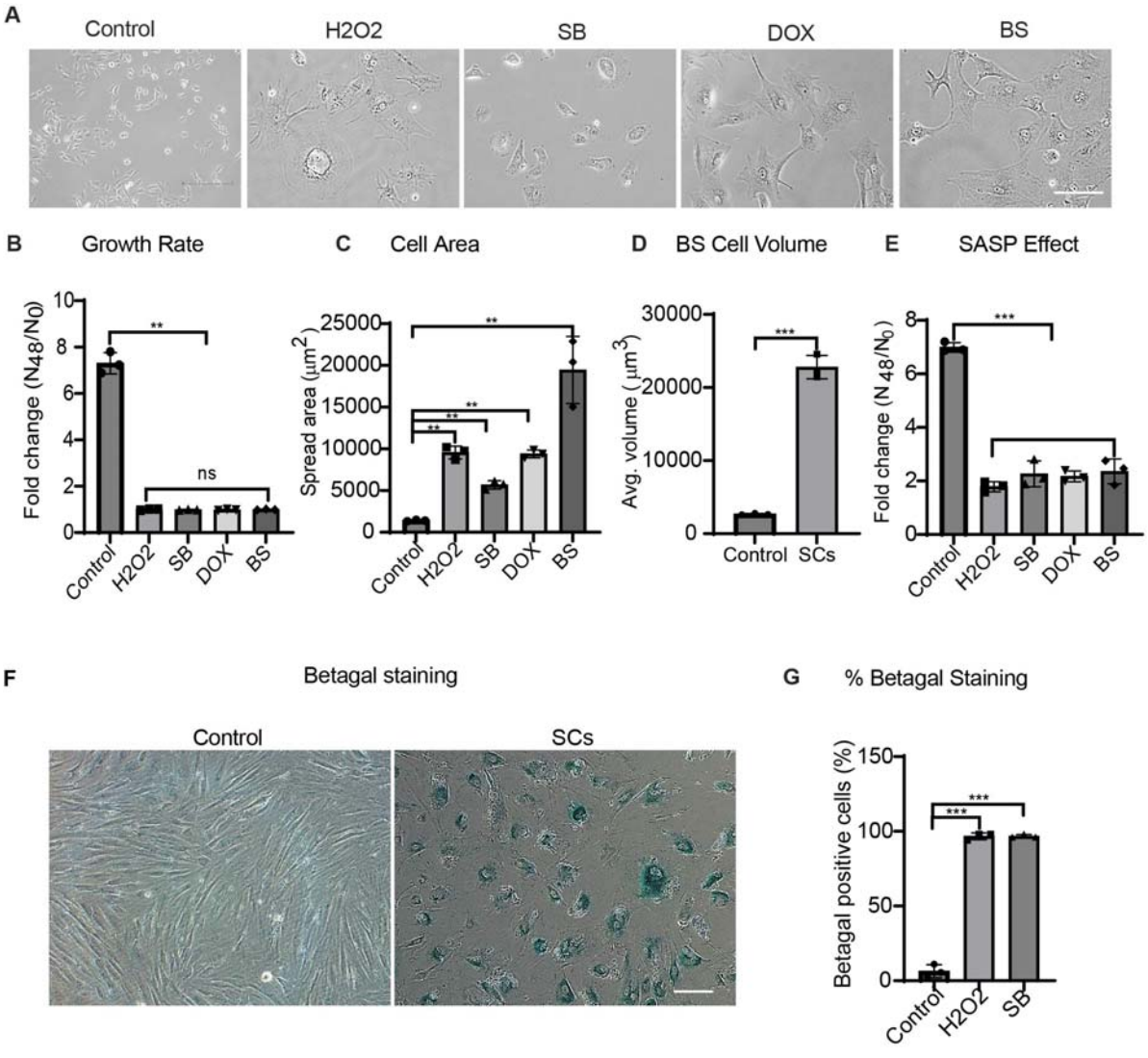

Figure 1 Characterization of Senescent Cells. (A) Brightfield images of control Vero cells and senescent cells

induced by H_2O_2, sodium butyrate (SB), Doxorubicin (Dox), and Bleomycin Sulphate (BS). Scale bar=300 µm. (B)

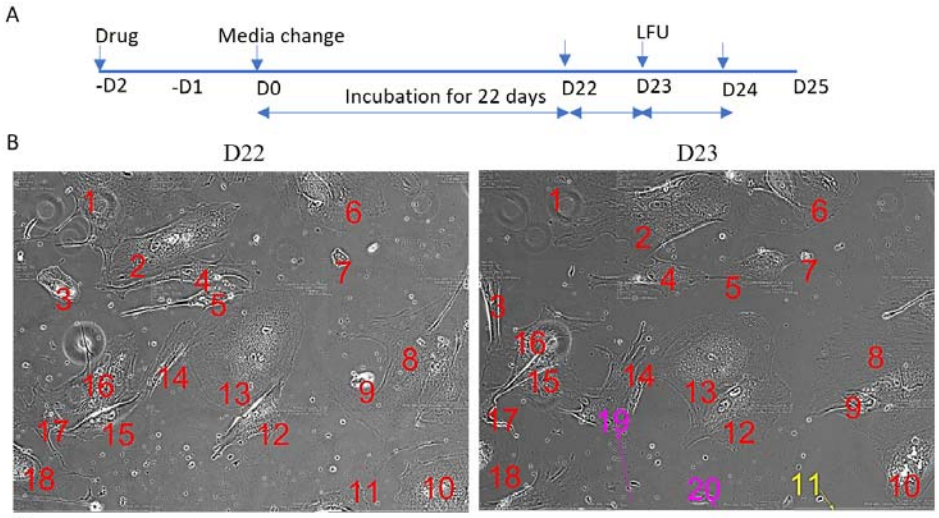

D

	Before LFU	After LFU
Begin Imaging	62	97
End Imaging	62	130

590 Quantification of proliferation shows no senescent growth after a 48 h incubation. (C) Senescent cells become enlarged

compared to the normal control cells. (D) Quantification of avg. cell volume of bleomycin sulfate treated cells compared to control cells. (E) Supernatant collected from the senescent cells after 24 hour incubation was used to study the growth of normal proliferating Vero cells. Culture medium was used as a positive control. Result are the

595 mean of three experiments ± SD. (F) SA-b-galactosidase staining of control (proliferating) and BS treated senescent cells. Scale bar= 300 µm. (G) Level of b-galactosidase senescence marker in H_2O_2 and SB induced SCs. Scale bar=300µm. *P<0.05, **P<0.002, *** P<0.0001;data in (B)-(E) and H are mean ± SD. Minimum of 150 cells were analyzed for spread area, cell volume and b-galactosidase from three independent experiments.

600

Figure 2. Fully Senescent Cells are Rejuvenated for Growth and Motility by LFU. (A) This diagram shows the

treatment plan to produce cells that are fully senescent. (B) Time-lapse video images of a field with 18 Bleomycin sulfate treated cells incubated for 22 days in vitro, at the beginning and end of ahour observation period (red numbers) where images were taken every 30' (two cells that entered the field in that period are marked by purple numbers and one that left by yellow). (C) Time-lapse images of a field of 14 cells after a 30' LFU treatment at the beginning and end of a 24 hour observation period (red numbers). Three of the orginal cells divided (#s 5, 8 and 13) and the daughter cells are noted by green numbers. Five cells entered the field (Purple numbers) and two left the fiel (yellow numbers). (D) Twenty-eight image fields were tracked for 24 hours before and for 48 hours after LFU treatment and the number of cells in those fields were counted.

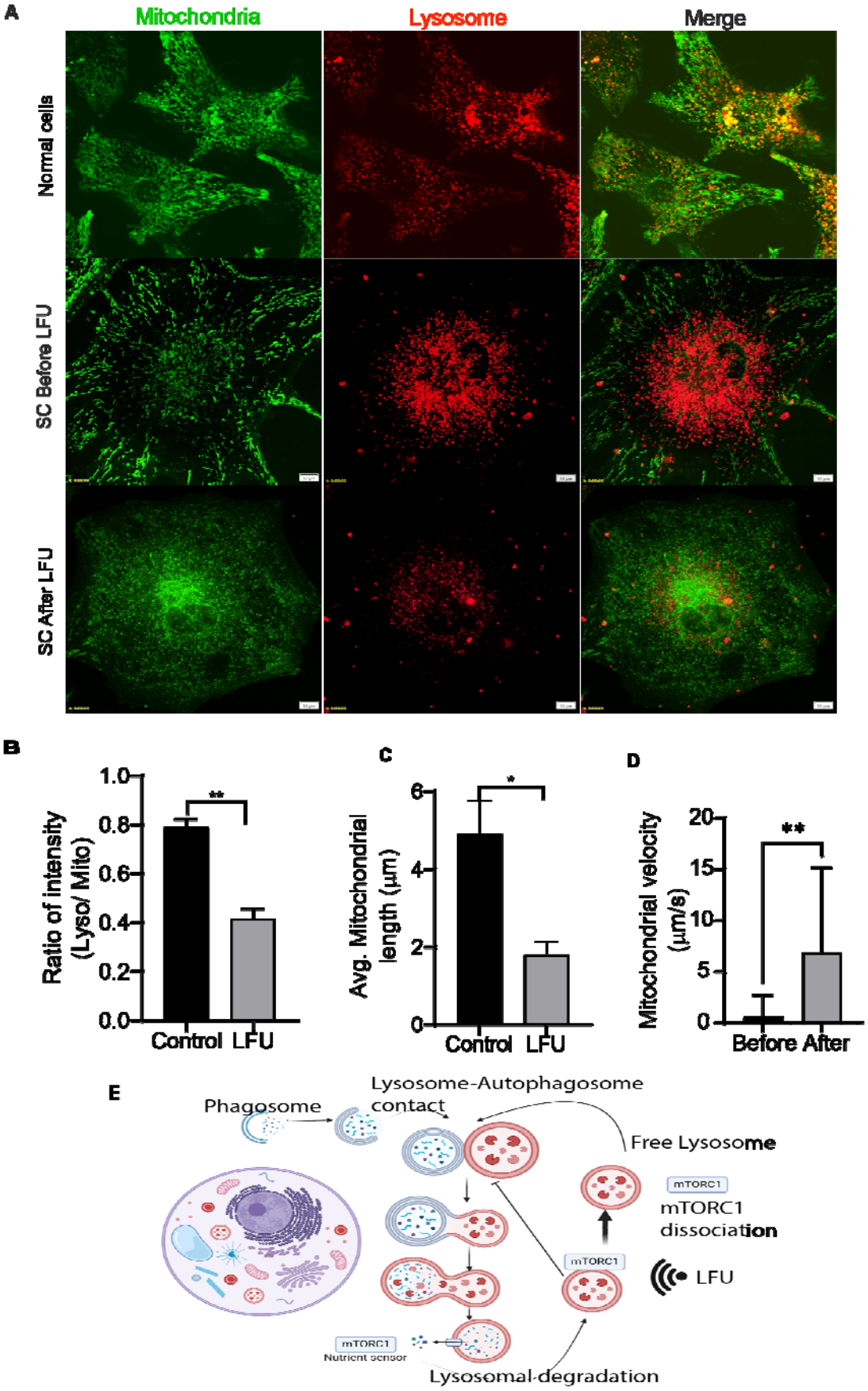

Figure 3 Low Frequency Ultrasound Decreases Mitochondrial Length and Lysosome intensity in Senescent Cells. (A) Representative immunofluorescent images of mitochondrial morphology and lysosome fluorescence in normal, senescent (bleomycin sulfate-treated for 30 hours and incubated for 3 days) and LFU-treated senescent Vero cells stained with Mitotracker and Lysosome tracker. Scale bar=10 µm. (B) Ratio of intensities of lysosomal to mitochondrial staining is decreased by ultrasound treatment of senescent cells. (C) Quantification of mitochondrial length shows decreased length after LFU. Results are shown as mean ± SD, minimally 108 cells were analyzed, n>3 experiments, and significance was determined using two-tailed unpaired t-test. *P<0.05, ** P<0.002. (D) Velocity of mitochondria before and after LFU treatment. Images were capture every five seconds for 10 minutes. A minimum of 10-12 mitochondrial puncta were manually tracking using ImageJ software. (E) Diagram of a working model for the rejuvenation of senescent cells by activation of autophagy through LFU inhibition of mTORC1 activity.

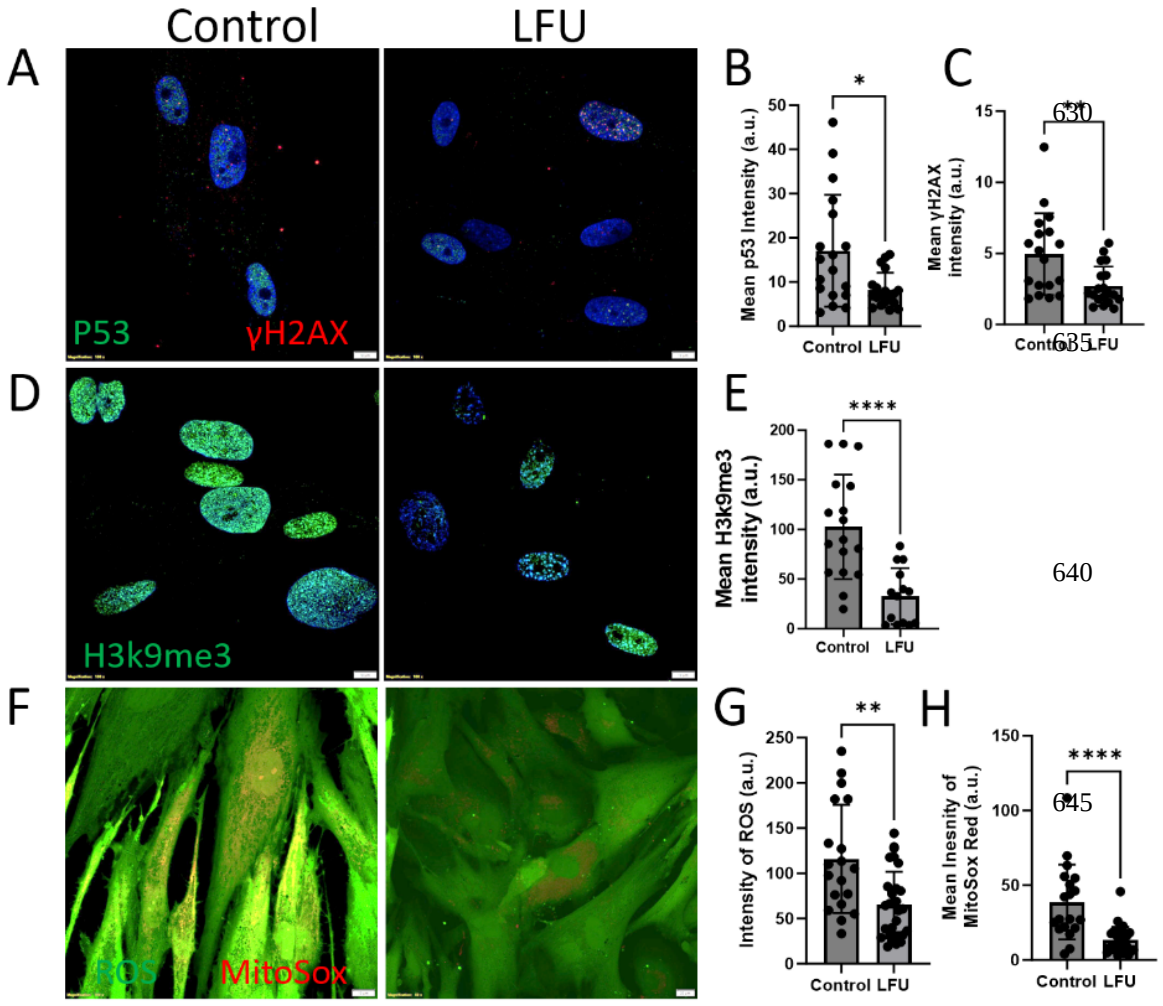

Figure 4. Senescence Markers in Senescent Cells Are Reduced after LFU Treatment. (A) Representative images of p53 (green) and γH2AX foci (red) stained cells. Sodium Butyrate senescent Vero cells were treated two times with or without LFU and then immunostained with P53 and γH2AX antibodies. Staining was done 24 hours after LFU treatment (2^{nd} treatment that was 1 day after first). (B) Quantification of p53 (green) intensity from the three replicates. (C) Quantification of γH2AX mean intensity from three replicates. (D) Representative images of H3k9me3(green) stained images. Sodium Butyrate senescent Vero cells were treated two times with or without LFU and then stained with H3k9me3 antibody (one day separated first and second LFU treatments and staining). (E) Quantification of H3k9me3 (green) intensity from the three replicates using standard conditions. (F) Representative images of ROS (green) and MitoSOX (red) treated cells with live cell staining probe. Sodium Butyrate induced Vero cells were treated with or without LFU and images were captured after 24 h. (G) Intensity of ROS (green) staining and (H) MitoSOX (red) staining from the three replicate experiments. Scale bar =10 μm. Data is plotted as mean± s.d. from the three replicates. One data point represents one cell analyzed. Non- parametric Mann Whitney test was used to determine the statistical significance between two groups. * p value<0.05, ** p value <0.007, **** p value<0.0001, and ns p value >0.05.

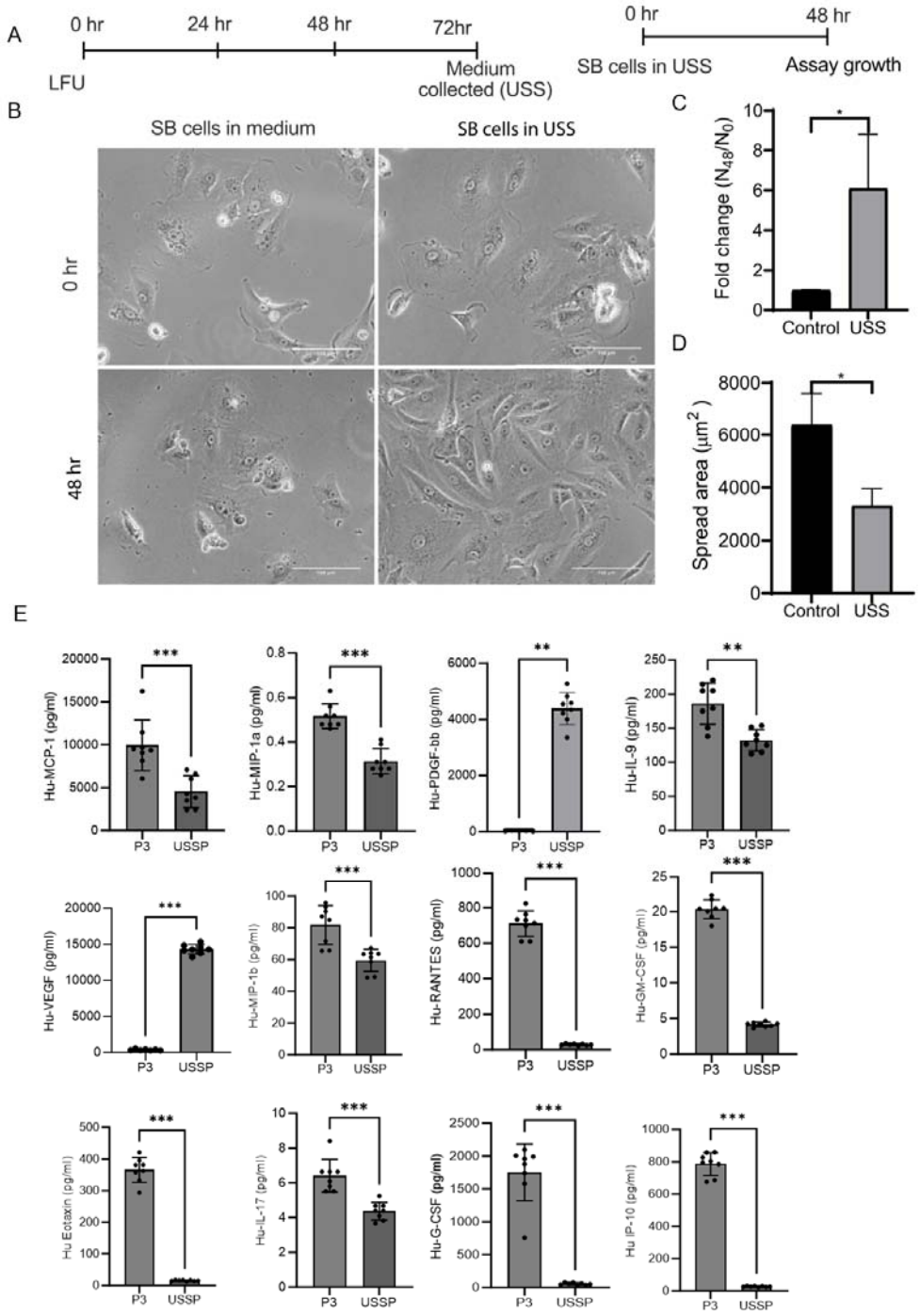

Figure 5 Normal Cells Treated with LFU Secrete Growth Activating Factors. (A) Timeline and strategy of LFU treatment of normal proliferating cells, passage 3 HFF cells. Schematic shows that normal cells were treated with LFU four times in the same media and the supernatant was collected (USS) for incubation with senescent cells for 48 h. (B) Brightfield images show change

in morphology of senescent cells in supernatant collected from LFU treated normal cells and after 48 h in the presence of USS. Senescent cells in normal growth medium were the controls. (C) Graph shows growth of SCs in USS increased and (D) shows decreased spread area of senescent cells. (E) Chemokines and cytokines in supernatants collected from untreated and LFU treated cells (P3 HFF) were analyzed using Multiplex immunoassay. Results are plotted as mean± s.d., n=6 replicates. Mann Whitney Test was used to determine the statistical significance, ns not significance, * p value <0.05 ** p value <0.01, *** p value 0.0001, and **** p value 0.00001. Graphs were plotted by mean ± SD; *P<0.05, **P<0.002, *** P<0.0001. Minimum, 200 cells were analyzed from the three independent experiments for graph (C) and (D). Scale bar= 300 µm.

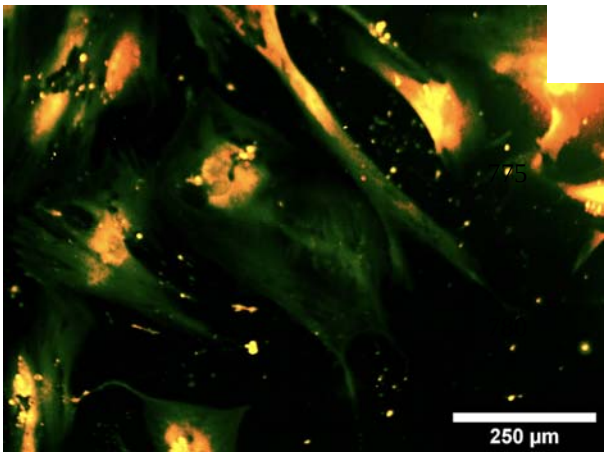

C

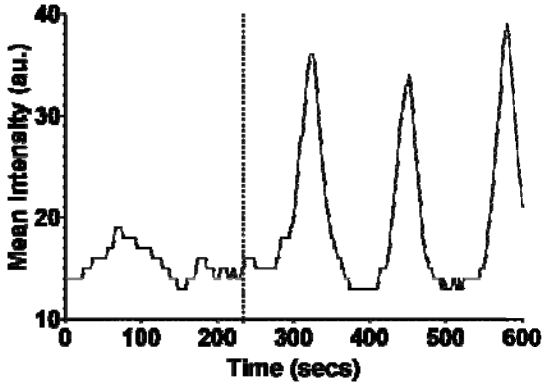

785

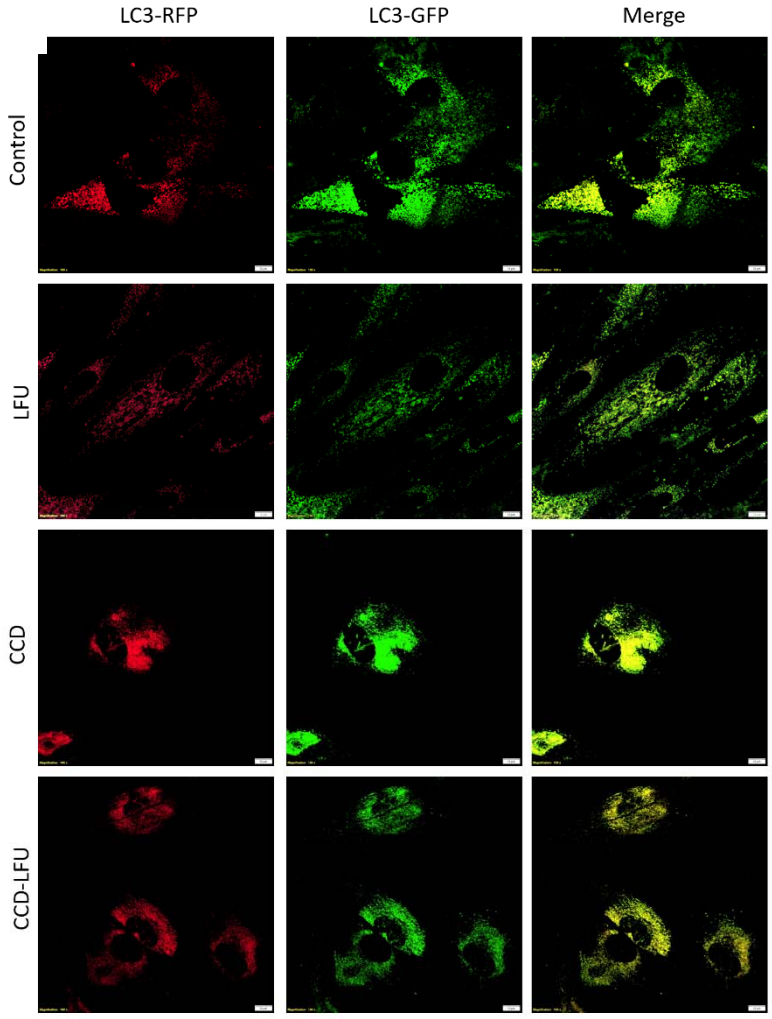

B

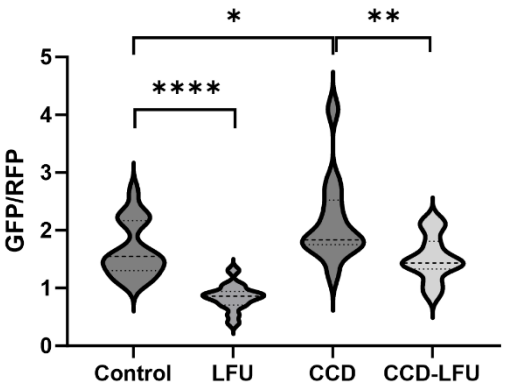

790

Figure 6: LFU Stimulates Ca2+ entry and Activation of Autophagy. (A) Ca^{++} indicator, calbryte 520 AM, fluorescence showing that LFU treatment for 2' causes a rise in Ca2+ levels in a large fraction of senescent cells. (B)

Time course of Ca^{++} levels in a senescent cell after LFU treatment starts at the vertical lined. (C) Representative immunofluorescence images of P18 HFF cells treated with LFU and treated with or without Chloroquine diphosphate (CCD, 10 Um). Control cells were not treated with CCD or LFU. Cells were transfected with autophagy sensor and incubated overnight as per manufacturer's instructions (See the method sections for details). Cells were then treated with CCD or LFU and incubated for 24 h. Confocal images were captured post 24 h incubation. Scale bar= 10 um. (D), violin plots show the quantification of mean intensity of LC3-GFP to LC3-RFP fluorescence. Autophagy flux is inversely correlated with GFP mean intensity because active autophagy quenches the GFP-LC3. Result is plotted as mean± s.d., n=80 fields ROI and a minimum 10 cells were analyzed. * p- value <0.05, ** p-value <0.01 and **** p value<0.0001, two tailed Mann Whitney test was used.

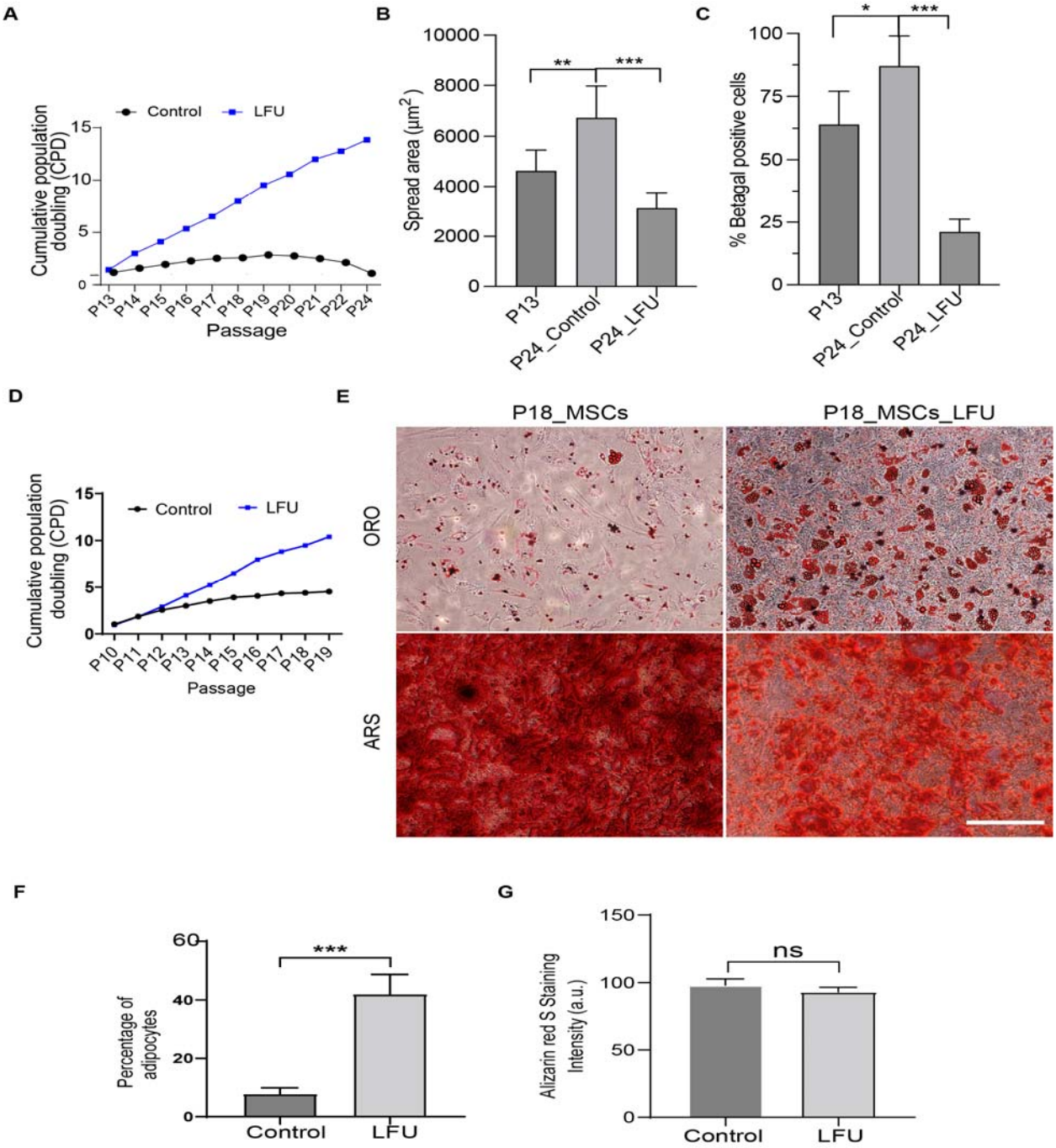

Figure 7 Ultrasound Reversal of Replicative Senescence Increases Number of Cells. (A) Growth rate shown as cumulative population doublings (CPD) for Control HFF and LFU treated HFF cells passaged every 48 h from P13 to P24 passage with LFU treatment every other passage (B). LFU treated cells were smaller than the p24 control and even p13 cells. (C) Percentage of SA-b-galactosidase positive cells decreased after LFU treatment. (D) Similarly, LFU treatment of mesenchymal stem cells (MSCs) expanded the cell number P10-P19, with treatment every other passage. (E) LFU treated MSCs showed normal differentiation to (ORO) adipocytes and (ARS) osteocytes. Oil red o staining dye marked lipid droplets (ORO) and alizarin red S-stained dye marked osteogenesis (ARS). (F) Percentage adipocytes were quantified in P18 MSCs treated with and without LFU. Results are plotted as mean of three

independent experiments, a minimum of 100 cells were counted. (G) Quantification of osteocytes was determined by the intensity of alizarine Red S staining. Mean intensity was calculated from ten random images of three independent experiments. Results are shown as mean ± SD, minimally 200 cells for spread area and 150 cells for percentage b-galactosidase analysis, n>3 experiments, and significance was determined using two tailed unpaired t-test. . *P<0.05, **P<0.002, *** P<0.0001.

Supplementary Materials

Materials and Methods

1. Cell lines and Cell Culture:

Human Foreskin Fibroblast (HFF) and Bone marrow derived mesenchymal stem cells were purchased from the ATCC. African monkey kidney derived Vero cells were obtained from the M. Garcia-Blanco lab as a gift. All these cell lines were cultured as per manufacturer's protocol. Vero cells and HFF cells were in growth medium containing Dulbecco's Modified Eagle's Medium (DMEM) 10 % fetal bovine serum (FBS; Gibco) and 1% Penicillin/ Streptomycin. Human MSCs were cultured in MSCs approved medium (ATCC) and expanded as per suppliers' protocol. Culture medium was changed in every 48 h unless otherwise stated. Cells plated at 20-40% confluency were maintained in an incubator at 37^0C and 5% CO_2. Cells were passaged every 48-72 h using Trypsin/EDTA (Gibco). Cells were counted manually using hemocytometer and ImageJ in at least three independent replicates unless otherwise stated. Minimally 5 fields were counted from each replicate.

2. MSCs Differentiation assays

LFU treated and untreated P18 MSCs were cultured in a 12-well culture plate in growth medium for 24 h. Then, growth medium was replaced by adipogenic (Invitrogen) and osteogenic (Invitrogen) differentiation media as per the manufacturer's protocol. Adipocytes were assayed after 12 days with oil red o (Sigma Aldrich) dye solution and osteocytes were assayed using Alizarin red S dye (Sigma Aldrich) solution. Images were acquired using a 10x evos RGB objective.

3. Senescence induction and quantification

Vero cells were treated with various stressors including 200 μM H_2O_2, 4 mM of sodium butyrate (SB), 25 mM of Bleomycin Sulphate (BS), 200 nM doxorubicin and incubated for 36-48 h. After washing with PBS and then adding fresh medium, cells were incubated for 4 days to confirm the growth arrest of senescent cells (*59*). Human foreskin fibroblast (HFF) cells were serially passaged until p15 since replication of these cells was dramatically reduced by p15-17. We used four criteria to determine if cells were senescent; (1) Cell cycle arrest by determining the growth rate, (2) Increase in cell spread area, (3) Development of senescence associated secretory phonotype (SASP) in culture medium, and (4) β-galactosidase staining. We captured images of cells with an Evos microscope at 10 X magnification after LFU treatment and 48 h post treatment. To measure growth by the increase in cell number, 15 random images were captured, then the average number of cells were determined, which was divided by the area of one frame to get the cell density (cells/cm^2). Then this seeding density was multiplied by the total area of the dish or well to obtain the total number of cells after LFU treatment and after 48 h if incubation. The total number of cells at 48 h was divided by the total number of cells just after LFU treatment to determine the growth rate. If the ratio was one, there was no growth.

Senescence was detected by the β-galactosidase senescence staining kit as per manufacturer's protocol. Briefly, sub-confluent senescent cells were stained by the SA-β-galactosidase staining solution and incubated overnight at 37^0C. The β-galactosidase-stained cells appeared blue and were Senescent cells. The percentage of β-galactosidase positive cells was determined by counting the number of blue cells and dividing by the total number of cells. Cell spread area was determined by capturing the images of cells with a 10X objective using an Evos microscope. Then, we used ImageJ software to calculate spread area by manually encircling the cell periphery of each cell. We used a minimum of 150 cells for the analysis. To determine the SASP activity, we cultured the senescent cells for 3-4 days and then supernatant was collected from each dish. This supernatant was used to culture normal cells. Development of a senescence phenotype by the normal cells in the supernatant medium confirmed that senescent cells were secreting SASP.

4. LFU treatment of cells

Prior to LFU treatment, the plates containing senescent Vero cells or late passage HFF cells were wrapped with parafilm to avoid contamination and water influx into the plate. The samples were placed on the plastic mesh, which was mounted on the water tank with an ultrasound transducer. Water in the tank was degassed and heated to 35^0C. The distance between the sample and transducer was approximately 9-10 cm. We also ensured that there were no

air-bubbles or air-water interfaces between the water and the sample. Output power of the transducer was measured at the plate location by a calibrated needle hydrophone (onda) . Cells were treated with pressure pulses of intermediate power and low frequency for 30 mins. Cells were treated with a 50% on-off duty cycle. After LFU treatment, cell plates were returned to the incubator for 48 h to determine the growth of senescent cells.

5. Reversal of senescence

First, we induced senescence in Vero cells using sodium butyrate, then we confirmed senescence using growth arrest and β-galactosidase staining after four days of incubation which normally got rid of quiescent cells (59). We treated the senescent cells using LFU with optimized parameters (power, frequency, and duty cycle). We incubated these cells for 48hr and we measured the growth and morphology of the cells before trypsinization. We named this passage P0. These cells were then trypsinzed, reseeded, and incubated for 48 hr. in the P1 passage. This process was repeated to P3 passage. We evaluated the cells in terms of fold change in number for growth, morphology, β-galactosidase, and EDU staining to check the population of senescent cells. Senescent cells without LFU treatment were used as control cells. Typically, by passage P3, the senescent cells exhibited the phenotype of normal proliferating cells.

Passage 15-24 HFF cells were treated with LFU at the optimized frequency and power. Cell proliferation was determined by counting the number of cells at the time of seeding and 48 h post LFU treatment. LFU treated HFF cells showed a higher growth rate than the untreated HFF cells. In the case of control P24 HFF cells, they were treated LFU and incubated for 96h prior to trypsinization, reseeding and incubation for 48 hours. Proliferation and morphology were measured after 48 of incubation. P24, LFU treated HFF cells became smaller in size, and they also showed dramatically greater proliferation than the untreated P24 HFF cells.

6. Soft surface preparation:

PDMS of 5 kPa elastic modulus was prepared by mixing the Sylgard 184 silicone elastomer kit at an Elastomer/curing ratio in 75:1. The combination was mixed, degassed and spin coated at 4000 rpm for 20 seconds on 27 mm ibidi glass bottom dishes. PDMS coated dishes were incubated at 65 °C overnight. Dishes were cleaned, activated by oxygen plasma treatment, then coated with 25 μg/ml Fibronectin (Sigma Aldrich) and kept overnight at 4 °C. Coated dishes were washed with PBS before plating the cells.

7. Microtubule analysis

Senescent cells were treated with tubulin tracker deep red (Invitrogen) as per manufacturer's protocol. Briefly, cells were incubated in tubulin tracker at 1000:1 for 30 min and medium was changed before confocal imaging with a 60x oil objective. The cells were treated with LFU and imaged again at the same confocal microscope settings. Length of myotubules was determined as described previously (Singh et al. 2021).

8. Pharmacological drug treatment

The following inhibitors were used in the study: Nocodazole (1μM), Cytochalasin D (100 nM), Blebbistatin (10 μM), Y27632 (1 μM), EX-527 (10 μM), GsMTx (1 μM) and Rapamycin (1 μM). Senescent cells were incubated in Resveratrol (100 μM) for 24 h to activate the Sirtuin 1 activity. L-Leucine (10 μM) and Rapamycin (200 nM) were used to activate and inhibit Phosphorylate mTOR during the 30 min LFU treatments. To assess LFU effect on TRPV1 activation or inhibition, we used Ruthenium Red (10 μM) and Capsaicin (10 μM) during the LFU treatments. For these treatments all inhibitors were purchased from Sigma Aldrich and prepared in DMSO and milli-Q water as per manufacturer's protocol. Cells were incubated in inhibitors overnight after 6-8 h cells seeding prior to LFU.

9. Senescence assay

Senescence was detected by the senescence associated β-galactosidase staining (Sigma Aldrich) as per manufacturer's protocol. Briefly, Senescent, non-senescent and LFU treated cells were seeded in 27 mm ibidi glass bottom dish and incubated for 48 h. Then, these cells were fixed and stained per manufacturer's protocol. After adding staining solution into the dish, cells were incubated overnight at 37°C in absence of CO2. A minimum of 100 cells were counted manually for each condition of the analysis.

Ten–15 random images were captured for each condition for analysis of β-galactosidase positive cells that were counted manually.

10. EDU and Annexin V staining

Cells were incubated with 10 mM EDU reagent for 24 h. Cells were then fixed, permeabilized and blocked according to the manufacturer's protocol (Click-iT EdU Alexa Fluor 555 imaging kit, Life Technologies). Hoechst was used to stain nuclei at a 5000:1 ratio. Images were captured with a 10X objective. The number of red puncta over the total number of blue nuclei gave the percentage of EDU positive cells. At least 200-300 cells were counted manually using ImageJ for each analysis. Apoptosis of senescent cells was determined using Annexin-V Alexa fluorophore 488 staining solution. Senescent cells were treated with LFU and after 30 mins, they were stained with

Annexin-V according to the manufacturer's protocol and imaged were taken in Evos microscope at 10X. Senescent cells treated with 0.5 mM H2O2 were used as a positive control.

11. Mitochondrial morphology

12. Ultrasound treated cells were incubated with Mitotracker (Invitrogen) at250 µM at 37°C for 30 min. Then, Images were captured in a Confocal microscope for quantification (15 randomized fields per sample). Mitochondrial velocity was determined from the time lapse image at the Olympus microscope at 60X. Images were captured after every 5 seconds for 10 minutes. Mitochondrial mobility was determined by the imageJ software with manual tracking. 10-15 mitochondria were traced manually. **Immunofluorescence staining**

Cells were fixed with 4% paraformaldehyde for 15 minutes, permeabilized with 0.5% Triton-X for 5 min, and blocked with 3% Bovine serum albumin (BSA) for 1 hour at room temperature and then incubated in primary antibody overnight at 4^0C. The following primary antibodies were used; rabbit polyclonal p21 antibody (cell signaling) (400:1), Mouse monoclonal p16 antibody (300:1) (abcam), Mouse H3k9me3 (500:1) (ThermoFischer), Mouse p53 (200:1) (SantaCruz Bio), Rabbit Gamma H2XA (200:1) (Cell Signaling), Mouse monoclonal SIRT1 antibody (300:1) (Sigma), P-mTOR, Ser 2448 (Cell-signaling D9C2) (200:1), Rabbit Anti YAP (ab52771)(300:1), α-Tubulin (ab7291)(500:1). After washing with PBS, cells were incubated with goat anti mouse 488 (1000:1) (Sigma) and Donkey anti rabbit 555 (1000:1) (Invitrogen) for 2 h. Nuclei were stained with Hoechst at 5000:1 dilution. Images were acquired by spinning-disk confocal microscope. Mitotracker green (Invitrogen) at 100 nM, Lysosome tracker deep red (Invitrogen) at 50 nM, and Tubulin tracker deep red 1000:1 were used as fluorescent tags.

Sodium Butyrate treated cells were incubated in MitoSOX Red (Invitrogen) and ROS probe (Dojindo's ROS Assay Kit) as per manufacturer's protocol. Briefly, Cells were treated with 5 mM of MitoSOX Red and 1:1000 ROS detection dye in HBSS for 30 mins. Then, cells were washed twice with HBSS and Treated with LFU and Cells were imaged at Olympus microscope using Ex/EM 490/520 and EX/EM 396/610 in controlled environment at 5% CO_2 and 37^0C.

Cytokine profiling by multiplex cytokine assay:

To analyze the level of chemokines, cytokines and immunoregulatory proteins in supernatant of LFU treated late passage and P3 HFF cells, we used Bio flex cytokines 27-flex kit assay (Bio-Rad). This multiplex immunoassay assay contained fluorescence nanoparticles conjugated with a specific antibody, and was used according to the manufacturer's protocol. Briefly, supernatant collected from the Late passage HFF and P3 cells treated with or without LFU, were diluted 1:4 and incubated for 2 h at room temperature in shaking. Then, wells containing samples were washed, and incubated with biotinylated antibody for 1 h at room temperature, then with streptavidin-phycoerythrin for another 30 min. A calibration curve was established using the standard given with the assay kit. Bioplex-200 plate reader (UTMB Galveston, Texas core facility) was used to assess the cytokine level. The concentrations of molecules were determined using the standard curve provided by the manufacturer.

Analysis of Autophagic flux:

To analyze the LFU induced autophagy in late passage HFF and in LFU treated HFF cells, we used Prema autophagy Tandem sensor RFP-GFP-LC3 kit (Invitrogen). Tandem sensor has acid sensitive GFP and acid insensitive RFP. In active autophagy, fusion of lysosomes with autophagosomes increased acidity, which quenched the GFP. Cells were cultured in 35 mm glass bottom dishes for 24 h before LFU treatment. Cells were transduced with autophagy tandem sensor according to the manufacturer's instructions. Briefly, 40 particles per cells were used for transduction, and incubated overnight in culture medium. Chloroquine diphosphate (100 μM) was used as an autophagy blocker overnight. Cells were visualized and images were captured at 100x on a spinning-disk confocal microscope (Olympus). Autophagy was determined as the ratio of intensities of GFP and RFP.

13. Telomere length measurement

The length of telomere was determined using Absolute Human Telomere Length Quantification qPCR Assay Kit (ScienCell AHTQL-8918) according to the manufacturer's protocol. Total genomic DNA was extracted from Human foreskin fibroblasts of various conditions including early passage (P2), late passage (P18) cells, LFU treated and untreated control cells using Invitrogen Pure Link Genomic DNA kit (K182001). 5 ng of genomic DNA was used as a template in PCR. Every experimental genomic DNA was processed four times. The reference DNA was analyzed in two triplicates. Telomere length was calculated according to the manufacturer's protocol.

14. DNA methylation assay

The protocol for DNA methylation was performed as reported previously (42). Cells were incubated in 20 µM CldU for 16 h. After trypsinization, cells were harvested and resuspended in ice cold PBS. A 2 µl droplet containing 200-300 cells was diluted in 8 µl of Lysis buffer (0.5% SDS, 50 mM EDTA, 200 mM Tris-HCl, pH 7.4). A 10 µl droplet containing cells diluted in Lysis buffer was poured onto the silane prepared slide (Sigma Aldrich), tilted, and allowed to flow by gravity. The slide was then fixed in methanol/ acetic acid (3:1) for 25-30 min and rinsed with PBS thrice. Slides were then denatured in 2.5 M HCl for 1 h; neutralized in 0.4 M Tris-HCl for 5 min and blocked in 5% BSA buffer for 1 h. Slides were stained with anti-BrdU (1:200) and 5mc (1:200) antibodies overnight at 4^{O}C. Slides were stained with Alexa flour 488 goat anti-rat (1:1000) and Q-dot 655 goat anti-mouse (1:2000) for 1 h for BrdU and 5mc antibody respectively.

15. RNA extraction and sequencing

RNA was extracted from early passage HFF cells (P2, P3, and P4) and rejuvenated senescent cells (P18, P19, and P20) using Qiagen RNeasy Mini Kit. (Germantown, MD). The UTMB Next Generation Sequence (NGS) core laboratory assessed RNA concentrations and quality using a Nanodrop ND-1000 spectrophotometer (Thermofisher, Waltham) and an Agilent Bioanalyzer 2100 (Agilent Technologies, Santa Clara, CA). PolyA+ RNA was purified from ~100 ng of total RNA and sequencing libraries were prepared with the NEBNext Ultra II RNA library kit (New England Biolabs) following the manufacturer's protocol. Libraries were pooled and sequenced on an Illumina NextSeq 550 High Output flow-cell with a single-end 75 base protocol. Reads were mapped to the human GRCh38 reference genome with STAR version 2.7.10a with the parameters recommended for the ENCODE consortium. Reads mapping to genes were quantified with the STAR –quantMode *(51)* GeneCounts option using the Gencode v41 (*52*) primary assembly annotation file. Differential gene expression was estimated with the DESeq2 software package, version 1.38.3, following the vignette provided with the package (*53*). The complete RNAseq data will be posted online.

16. Statistical analysis

All results are shown as mean ± s.d. and two-tailed unpaired t-test, Mann Whitney tests, and Kruskal Wallis One way

ANOVA test followed by post hoc Dunn's test was used to determine the statistical significance between two groups.

GraphPad Prism 8.4.3. was used for making graphs and statistical analyses. * P values<0.05, ** p values< 0.002, ***

1010 p values <0.001, ****< p value 0.0001 and non-significant (ns) p-value >0.05 were used, shown in the figures.

1015 Table 1 RNAseq Data

List of Upregulated Genes in LFU Rejuvenated HFF vs Senescent Cells			
S. No.	**Name**	**log_2FoldChange**	**P-value**
1	IFI27	4.706732879	3.39E-139
2	ANO3	4.303317562	7.94E-19
3	BST2	4.267516399	4.60E-48
4	NGFR	4.227721006	3.99E-15
5	OAS1	4.194394186	2.58E-109
6	OAS2	3.851520822	3.19E-205
7	IFI6	3.687238684	0
8	NTSR1	3.587703179	5.84E-20
9	MX1	3.41456665	7.56E-188
10	MX2	3.353896447	4.53E-85
11	IFITM1	3.267590391	1.12E-82
12	SFRP1	3.062130153	1.02E-136
13	OAS3	3.039643219	3.46E-89
14	RSAD2	3.00663542	9.46E-26
15	CMPK2	2.992910736	4.73E-32
16	EDARADD	2.971533613	5.08E-10
17	GBX2	2.893735519	9.38E-11
18	ENSG00000225886	2.869460744	7.25E-07
19	NEURL3	2.844376063	2.79E-05
20	SLC38A11	2.839565113	1.67E-59
21	SPHKAP	2.79074685	1.05E-25
22	ESM1	2.774304098	1.52E-48
23	HAS2	2.761341752	1.28E-48
24	HSPA6	2.608245534	3.99E-10
25	CCL5	2.545666491	1.38E-20
26	HERC6	2.543077514	5.23E-87
27	LINC01234	2.475565502	4.77E-08
28	ANGPT2	2.472972104	2.32E-05
29	TMEM158	2.442808274	2.10E-59
30	DIRAS3	2.426571346	4.54E-09
31	IFI44	2.382909102	1.83E-78
32	EPSTI1	2.376583283	1.42E-66
33	ZNF385D	2.372390644	4.42E-10
34	STAC	2.368386566	1.66E-11
35	GBX2-AS1	2.334084241	5.12E-07
36	GNA15	2.318072578	2.24E-06
37	IFI44L	2.303837053	5.65E-37
38	HERC5	2.285450475	4.55E-44
39	COLEC12	2.264077281	2.70E-15
40	ISG15	2.259660967	5.02E-145
41	ANO9	2.258562492	7.43E-05
42	FRMD3	2.243609765	1.57E-27
43	CD36	2.218190589	1.51E-15
44	IFIH1	2.192859031	1.26E-42
45	HAND2	2.127703818	3.13E-19
46	BLK	2.055308732	3.31E-05
47	IFIT1	2.051756712	1.68E-146

48	USP18	2.047027284	8.39E-32
49	SLC24A3	2.035592849	1.77E-45
50	OASL	2.029842409	1.58E-21
51	LRRC37A6P	2.02025571	1.49E-06
52	PODXL	2.016215331	1.31E-35
53	EPB41L3	2.000835065	5.10E-127

1020

Table 2:

List of Downregulated Genes in LFU Rejuvenated HFF vs Senescent Cells			
S. No	**Gene**	**log2FoldChange**	**P-Value**
1	EMX2	-6.685669619	4.98E-16
2	EMX2OS	-6.092350389	1.33E-20
3	RSPO3	-5.647577153	2.01E-10
4	TCF21	-5.453748247	2.25E-11
5	KRT7	-5.380677243	0
6	LRRC61	-5.292511308	1.49E-09
7	IRX1	-5.234068069	1.33E-10
8	TBX4	-5.02798295	1.63E-38
9	KCNH2	-4.911524296	4.44E-08
10	SLC38A5	-4.79985076	7.19E-84
11	LRFN5-DT	-4.591846467	4.13E-07
12	STK26	-4.584984891	6.92E-27
13	ACTR3C	-4.533911714	3.85E-07
14	GFRA1	-4.507783777	7.78E-100
15	NLGN4X	-4.436825012	7.01E-07
16	CLDN11	-4.380720667	1.40E-41
17	CNTN3	-4.258840807	5.35E-49
18	CHRM2	-4.210605354	1.86E-144
19	EFEMP1	-4.210109619	0
20	PIEZO2	-4.186528467	4.15E-20
21	POSTN	-4.180979239	1.51E-79
22	KCNJ6	-4.143034445	1.17E-06
23	ACP3	-4.141166627	1.53E-35
24	SPESP1	-4.099375016	7.32E-30
25	HOXD13	-4.087047929	9.71E-18
26	EBF1	-4.078835958	5.72E-24
27	ADGRD1	-4.053786369	7.49E-50
28	CES1	-4.051421755	3.36E-08
29	ALX3	-4.049073332	1.04E-24
30	HOXD12	-3.960130505	2.80E-06
31	FOXP2	-3.894518884	2.92E-10
32	CDH6	-3.883670483	1.09E-36
33	TAFA5	-3.769737561	9.67E-15
34	LINC01397	-3.764559924	1.07E-21
35	PCDHGA12	-3.74039003	9.13E-81
36	KCNQ3	-3.658171387	6.54E-41
37	C1QTNF7	-3.653338267	8.27E-06
38	PDE9A	-3.642856719	1.79E-09
39	SIX2	-3.626917422	7.83E-32
40	CLEC2B	-3.620247018	4.59E-99

41	FOXL2NB	-3.565501153	8.61E-75
42	LRFN5	-3.540521045	1.27E-05
43	LRATD1	-3.501612735	2.73E-63
44	ZNF804A	-3.485363219	4.03E-70
45	LINC01391	-3.473586864	2.91E-11
46	ENSG00000286023	-3.46713835	1.44E-05
47	MAF	-3.445540321	3.58E-44
48	ZNF536	-3.41991169	1.37E-16
49	FGF7	-3.410329734	2.50E-118
50	ZBED10P	-3.363205368	1.19E-08
51	SLCO3A1	-3.35068457	1.20E-66
52	LINC00968	-3.332697292	3.01E-84
53	WNT2	-3.310466489	3.61E-26
54	UBL4B	-3.265322281	4.50E-18
55	GRID1	-3.247459554	4.93E-10
56	SYBU	-3.18364944	5.47E-12
57	KYNU	-3.1772595	9.03E-37
58	HTR2B	-3.162738129	2.22E-08
59	TACR1	-3.123747595	1.21E-34
60	LINC02575	-3.121696951	3.02E-05
61	GSTM5	-3.107487362	4.52E-44
62	LSAMP	-3.106013169	4.34E-07
63	CACNA1H	-3.105263645	2.36E-16
64	CYP1B1	-3.056180785	3.28E-72
65	SPATC1L	-3.04033194	3.04E-82
66	ALDH1A1	-3.030498204	1.53E-46
67	ZNF608	-3.019061524	8.08E-31
68	BDKRB1	-2.982299496	7.48E-68
69	FOXL2	-2.930627548	5.00E-88
70	LRRC38	-2.926345364	2.71E-08
71	PGM5	-2.907450315	2.83E-16
72	HR	-2.882876872	1.59E-16
73	KLHL13	-2.858644818	8.81E-07
74	AKR1B10	-2.828515048	2.57E-20
75	LRRK2	-2.813294912	6.63E-28
76	ZNF812P	-2.804622944	5.40E-05
77	RSPO4	-2.80077542	1.04E-12
78	MBNL3	-2.772589763	1.01E-12
79	CEMIP	-2.772163949	3.24E-42
80	AJAP1	-2.759826982	1.11E-78
81	PITX1	-2.753771797	8.90E-157
82	CTHRC1	-2.75249351	2.57E-166
83	PDE3B	-2.751121655	2.01E-08
84	NETO1	-2.737809763	1.12E-13
85	DNAH11	-2.728034879	4.57E-32
86	KCNN2	-2.714670274	5.67E-51
87	ELAPOR2	-2.652372937	1.77E-05
88	MEOX2	-2.645123188	5.06E-05
89	PCDH7	-2.634530158	1.12E-27
90	SESN3	-2.558015787	1.64E-09

91	SELENOP	-2.557147353	1.24E-06
92	SMIM43	-2.541340191	6.34E-23
93	HOXD11	-2.523786445	3.27E-45
94	DGKI	-2.500401863	3.50E-96
95	HEPH	-2.475523638	1.32E-22
96	IGFBP2	-2.466853867	1.12E-63
97	SLC22A3	-2.46160273	9.84E-05
98	SLC7A2	-2.433374832	1.05E-18
99	TENT5C	-2.432640797	1.15E-54
100	GASK1B-AS1	-2.429532141	4.79E-25
101	EPHB2	-2.422231395	9.03E-73
102	USP32P1	-2.420897639	0.000104623
103	LINC00470	-2.409567901	0.000108628
104	NPTX1	-2.409035393	2.96E-15
105	ZFPM2	-2.407235333	1.07E-12
106	ENSG00000272622	-2.394920051	3.07E-13
107	SCIN	-2.389771086	9.16E-43
108	SPP1	-2.387033205	1.33E-46
109	IP6K3	-2.386317917	3.56E-26
110	CARD16	-2.356929744	4.07E-07
111	EYA1	-2.34786137	8.11E-17
112	MEDAG	-2.342822386	5.37E-08
113	IGF2	-2.342163551	3.46E-124
114	TRABD2A	-2.335635088	5.16E-41
115	CYTL1	-2.312629587	1.85E-09
116	PDPN	-2.299643651	1.57E-67
117	SCG5	-2.299180836	1.84E-12
118	SOX5	-2.291381027	1.93E-12
119	BMP2	-2.290319768	1.57E-89
120	SPATA22	-2.289593656	0.000139229
121	PTPRD	-2.286131544	1.28E-08
122	PTPN20	-2.282776934	6.58E-06
123	PRKG2	-2.216841137	2.63E-06
124	LRP1B	-2.19440983	3.01E-06
125	FOXL1	-2.163990518	2.36E-44
126	ALDH1L1	-2.160436746	5.69E-05
127	TSPAN2	-2.130477479	4.36E-19
128	RGN	-2.124685546	1.31E-11
129	LAMC3	-2.119262696	6.71E-08
130	IGF2-AS	-2.117221411	8.75E-05
131	MSC	-2.108497484	1.84E-60
132	TREML3P	-2.057728892	6.84E-13
133	GABRB3	-2.054842442	1.51E-07
134	COL11A1	-2.050412705	1.05E-44
135	CADPS	-2.032686913	8.18E-05
136	RPL7AP28	-2.022183902	9.37E-06
137	ADA2	-2.013230344	3.74E-14
138	GLDN	-2.004207555	1.02E-06
139	ARNT2	-2.000734631	8.75E-75
140	MCTP1	-2.000477258	5.16E-14

1025 Table 3: List of Genes upregulated in LFU treated late passage HFF cells.

Bio Process	p-value	q-value	overlap_genes
Influenza A	1.619929e-08	9.881566e-07	[IFIH1, RSAD2, OAS1, OAS2, MX2, OAS3, CCL5, MX1]
Measles	7.942201e-08	2.422371e-06	[IFIH1, OAS1, OAS2, MX2, OAS3, MX1, HSPA6]
Hepatitis C	1.828574e-07	3.718100e-06	[RSAD2, OAS1, OAS2, MX2, OAS3, MX1, IFIT1]
Coronavirus disease	2.527530e-06	3.854483e-05	[IFIH1, OAS1, OAS2, MX2, OAS3, MX1, ISG15]
NOD-like receptor signaling pathway	1.344502e-03	1.640292e-02	[OAS1, OAS2, OAS3, CCL5]
Herpes simplex virus 1 infection	1.970480e-03	1.750871e-02	[BST2, IFIH1, OAS1, OAS2, OAS3, CCL5]
Epstein-Barr virus infection	2.009196e-03	1.750871e-02	[OAS1, OAS2, OAS3, ISG15]
Human papillomavirus infection	1.141362e-02	8.702885e-02	[MX2, MX1, ISG15, OASL]
RIG-I-like receptor signaling pathway	1.483205e-02	1.005283e-01	[IFIH1, ISG15]
Lipid and atherosclerosis	1.935232e-02	1.180492e-01	[CCL5, HSPA6, CD36]

Table 4: List of Genes downregulated in LFU treated late passage HFF cells.

Bio Process	p-value	q-value	overlap_genes
GnRH secretion	0.001055	0.119259	[KCNJ6, SPP1, KCNN2, CACNA1H]
Calcium signaling pathway	0.006934	0.309739	[CHRM2, FGF7, HTR2B, BDKRB1, TACR1, CACNA1H]

Serotonergic synapse	0.008223	0.309739	[GABRB3, KCNJ6, HTR2B, KCNN2]
Regulation of actin cytoskeleton	0.018747	0.394402	[CHRM2, ACTR3C, FGF7, SCIN, BDKRB1]
GABAergic synapse	0.024628	0.394402	[GABRB3, KCNJ6, SLC38A5]
Morphine addiction	0.026083	0.394402	[GABRB3, KCNJ6, PDE3B]
Circadian entrainment	0.030721	0.394402	[KCNJ6, PRKG2, CACNA1H]
Neuroactive ligand-receptor interaction	0.033034	0.394402	[CHRM2, GABRB3, GRID1, HTR2B, BDKRB1, TACR1]
Pathways in cancer	0.033440	0.394402	[ARNT2, FGF7, BMP2, LAMC3, IGF2, BDKRB1, WNT2, GSTM5]
Tryptophan metabolism	0.034903	0.394402	[KYNU, CYP1B1]

Supplemental Figures

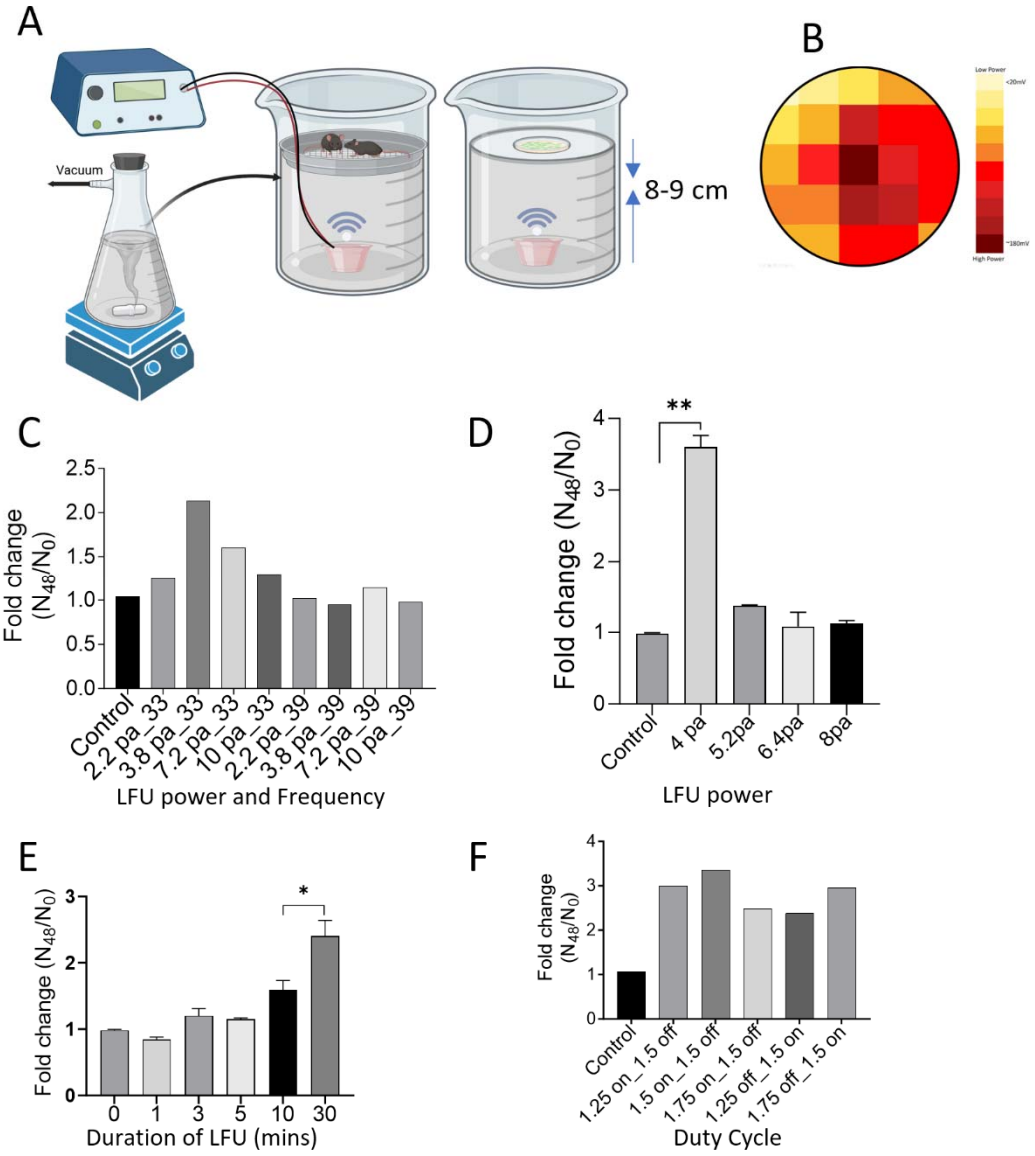

Figure S1 Schematic of LFU experiment setup and optimization of treatment parameters. (A)Schematic of LFU treatment setup for cells and mice. (B), Heat map representing the distribution of LFU output power at the location of treatment, darkest red shows the maximum output power measured by the hydrophone and the yellow color shows the minimum output power. (C), Bar graph showing the growth of Sodium butyrate senescent Vero cells in 48h h after LFU treatments with various power levels at 33 & 39 kHz. Data is represented as the mean of three replicates. (D), Bar graph representing the growth of SCs in 48 h after 33 kHz LFU treatment at the designated power level. Data is represented as the mean ± s.d. of three independent experiments. ** p- value < 0.01 by unpaired two tailed student t-test. (E), Growth was determined as a function of the LFU treatment duration. Control represents no LFU treatment. Results plotted are the mean of three independent experiments ± s.d. *p value <0.05 by unpaired two tailed student t-test. (F)**,** Effect of duty cycle on growth. Results plotted are mean of 3 replicates.

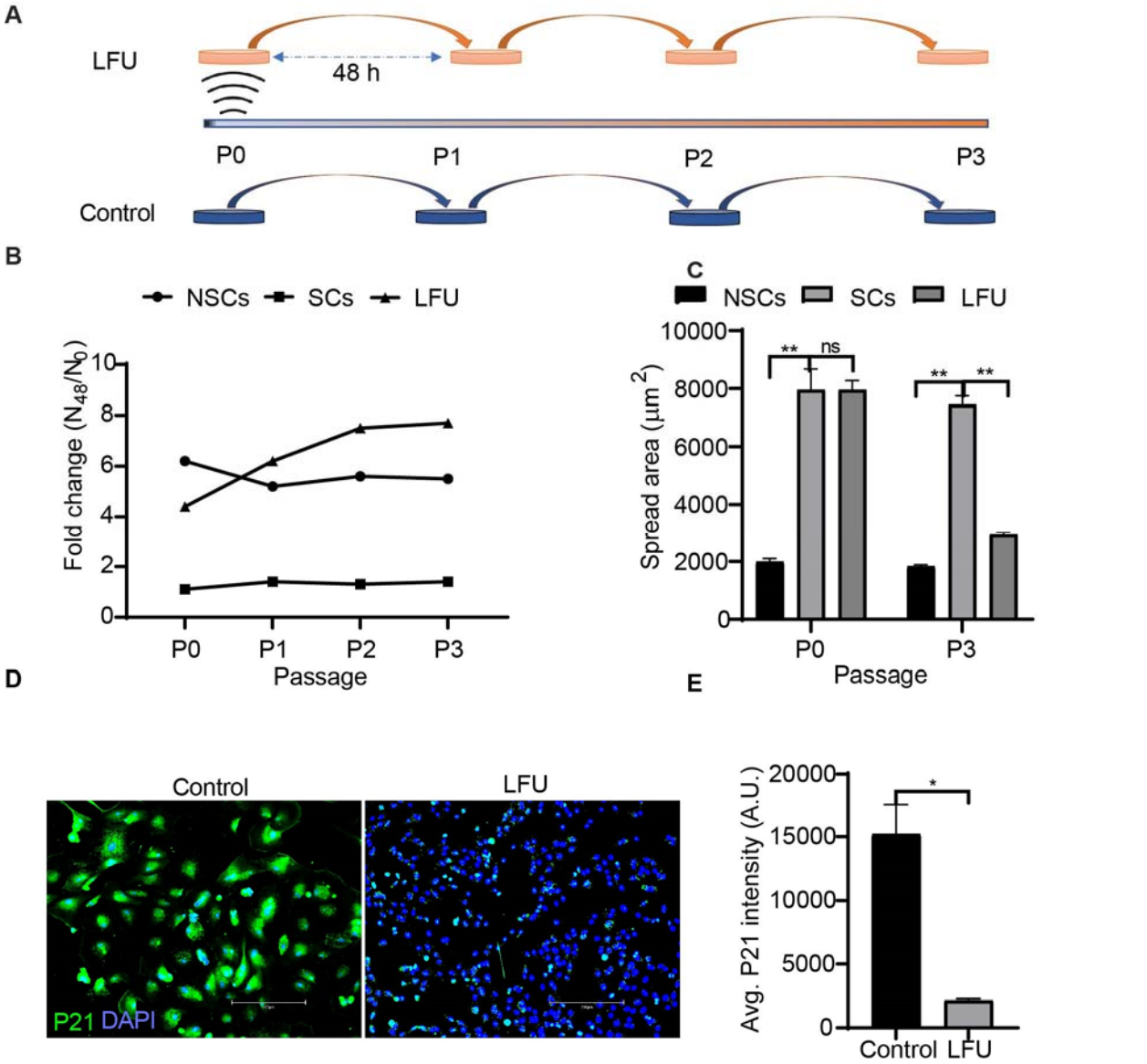

Figure S2 Ultrasound Reverses Cell Senescence. (A) Schematic illustration showing experiment design of LFU induced reversal of senescence after Sodium Butyrate (SB) treatment for 48 hour followed by incubation for 4 days. (B) Growth of Sodium Butyrate (SB) treated senescent Vero cells after low frequency ultrasound (LFU) treatment and passaged every 48 h for 8-10 days. NSCs were the non senescent Vero cells Graph shows growth of normal Veros (NSC), BS senescent (SC) and LFU treated (LFU) senescent cells as fold change over 48 h for passages from P0 to P3 every 48 h. (C) Cell area of LFU treated senescent cells (LFU) is largely restored to normal by P3. (D) Representative anti-p21 immunofluorescence images of senescent P3 control and LFU treated senescent P3 cells. Scale bar= 300 µm. (E) Quantification of fluorescence intensity of p21 stained senescent and LFU treated senescent P3 cells shown as mean ± SD, for >200 cells in each condition. All graphs were plotted by mean ± SD and p values ns $p>0.05$, *$P<0.05$, ** $P<0.002$. Minimum 200 cells were analyzed from three independent experiments in each condition.

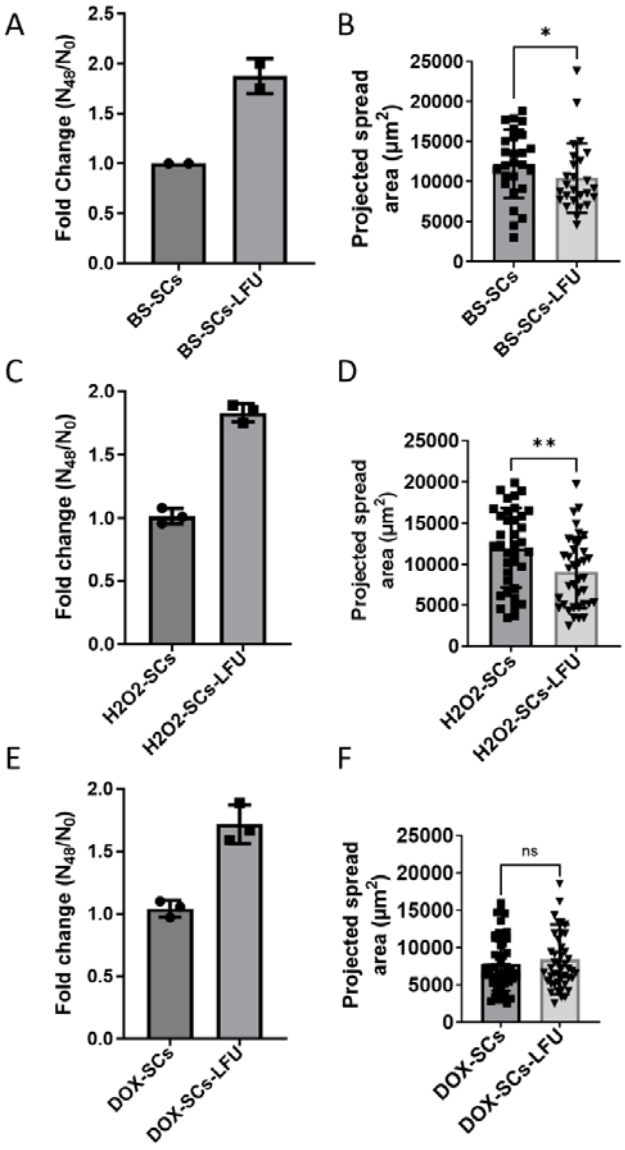

Figure S3: LFU treatment activates growth and reduces cell size of drug-induced senescent Vero cells. (A) Growth of Bleomycin Sulphate (BS) (50 µM) induced senescent cells treated once with or without LFU after 48 h. (B) Spread area of BS cells was measured before trypsinization 48 hour after LFU or no treatment, by analyzing the brightfield images. (C) Graph showing growth of H_2O_2 (200 µM) senescent cells with LFU or no treatment after 48 h. (D) Spread area of H_2O_2 was measured after 48 h from captured images just before the trypsinization. (E) Growth of Doxorubicin (200 nM) induced senescent cells with no or LFU treatment after 48 h. (F) Spread areas of Doxorubicin induced senescent cells were measured 48 h after LFU treatment. Results are plotted as mean of three replicates and ± s.d. At least 35-50 random cells were analyzed from the three replicates. Non-parametric Mann Whitney test was used to determine the statistical difference between the two groups. * p value <0.05. ** p value<0.001 and ns p value >0.05.

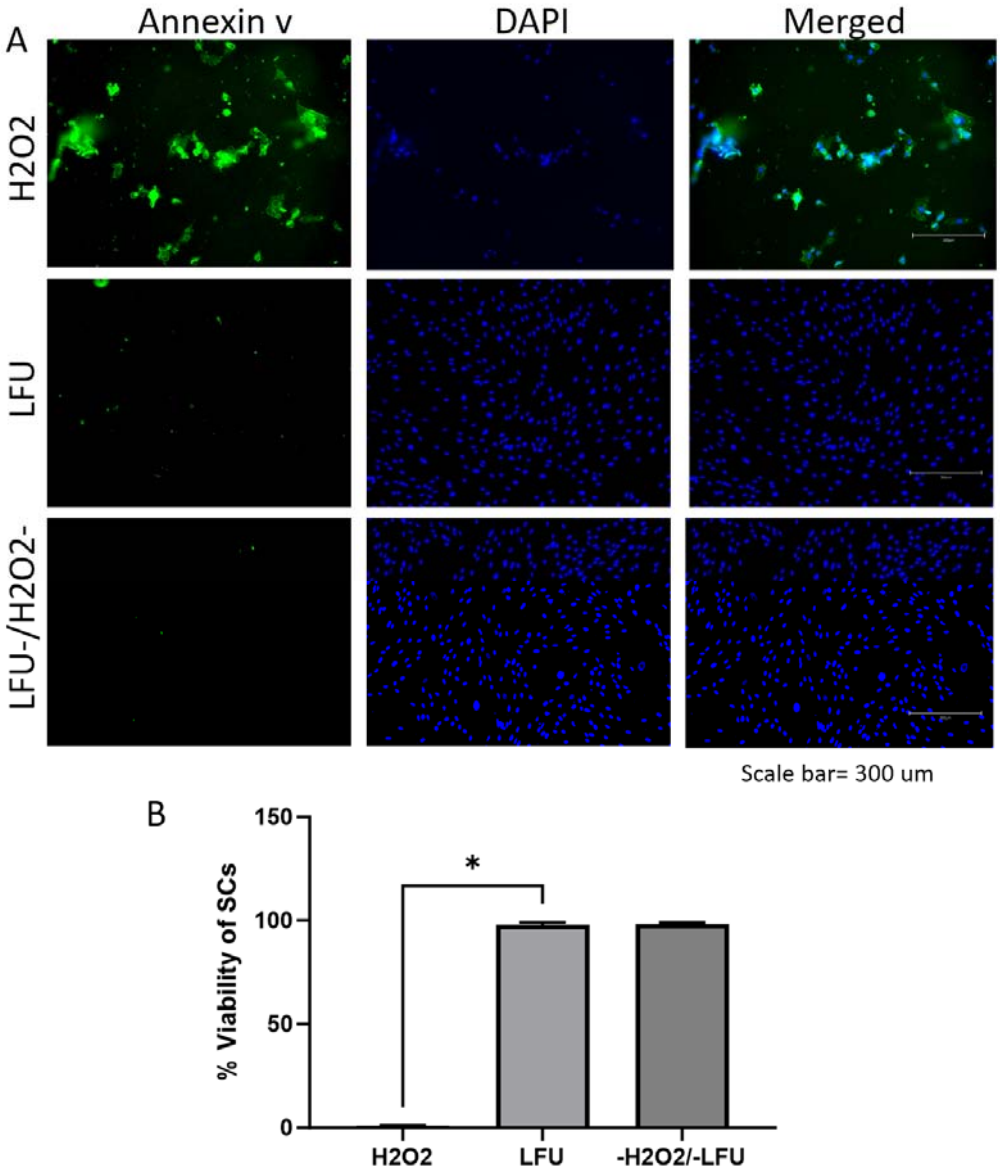

Figure S4 : LFU treatment of Senescent cells Does not Cause Apoptosis. (A) Immunofluoresecnce images of P13 HFF cells treated with 500 μM hydrogen peroxide (H_2O_2) to induce apoptosis as positive control. Alternatively, 50 mM of H_2O_2 was used to induce senescence; and after 2 days of incubation, LFU-/H_2O_2 cells were treated for one hour with LFU. As a negative P13 cells were treated for one hour with LFU. LFU treated cells were assayed for apoptosis with an Annexin V assay after one hour (see Materials and Methods). Although all cells treated with 0.5mM H_2O_2 bound Annexin V, neither the P13 controls nor the 50 mM H_2O_2 cells showed Annexin V staining. (B) Quantification of images was performed by manually counting the number of cells stained with Annexin and DAPI and dividing by the number of DAPI cells. More than 400 cells were counted for each condition. Experiment was performed in triplicate. Results are plotted as mean ± S.D; *P<0.05, unpaired t-test was used to determine the p value.

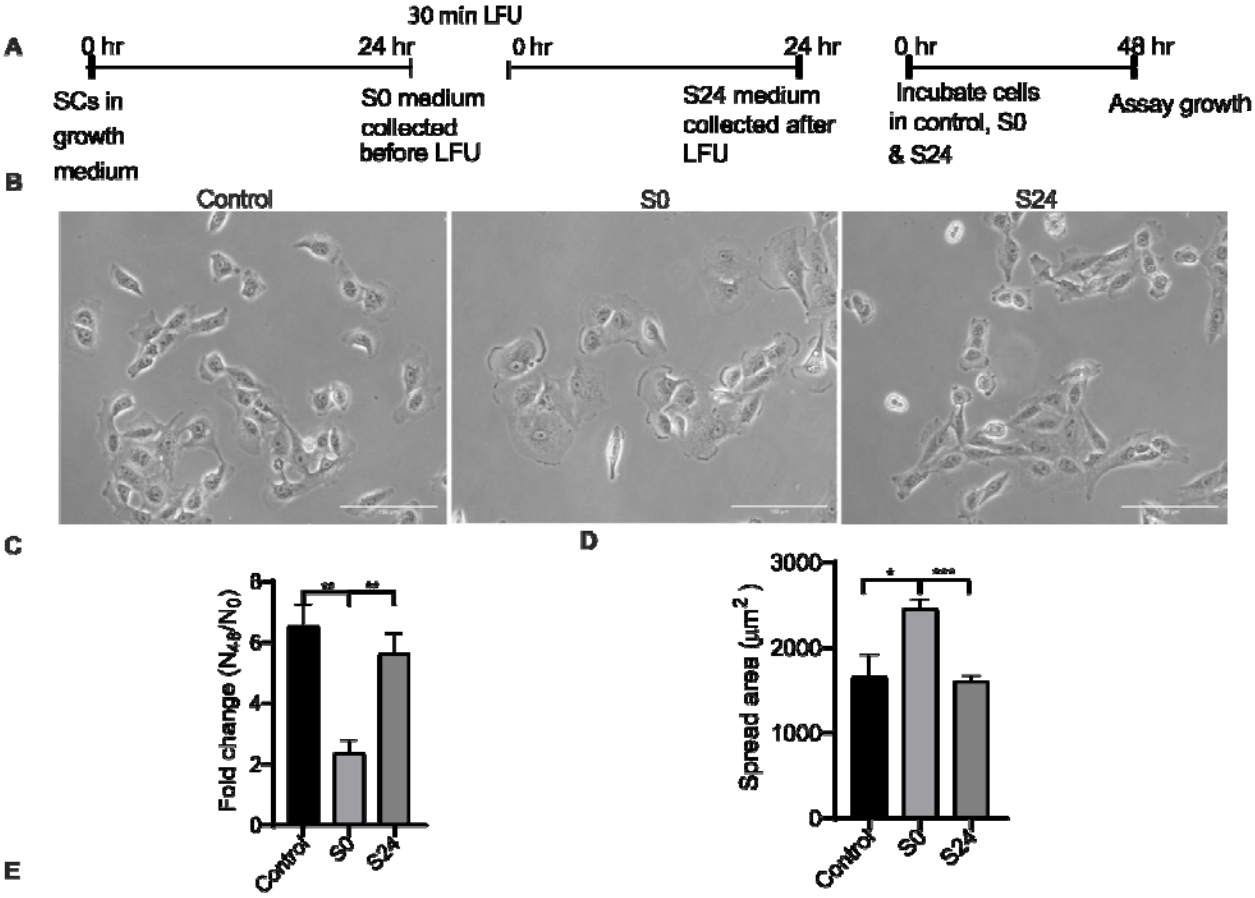

1215

Figure S5: LFU Treatment Causes Decreased SASP Secretions . (A) Schematic illustration of the experiment. BS senescent cells were cultured in growth medium for 24 hr and then they were treated with low frequency ultrasound (LFU) for 30 min. Supernatant was collected after the LFU treatment (S0) and cells were incubated for another 24 hour in fresh medium before supernatant was collected after (S24). To check the effect of LFU treatment, supernatants S0 and S24 were used to check the growth of non-senescent HFF cells. (B) Representative brightfield images of control cells after 48 hours of incubation in normal growth medium, S0, and S24. (C) Quantification of control cell numbers and (D) cell areas after 48 in control, S0 or S24 supernatants. (E) Chemokines and cytokines in supernatants from untreated and LFU treated Late passage HFF (P19) cells were measured using Multiplex assay before and after LFU treatment. Results are plotted as mean± s.d., n= 6 replicates, ns not significance, * p value <0.05 ** p value <0.01, *** p value 0.0001, and **** p value 0.00001 using Mann Whitney Test.

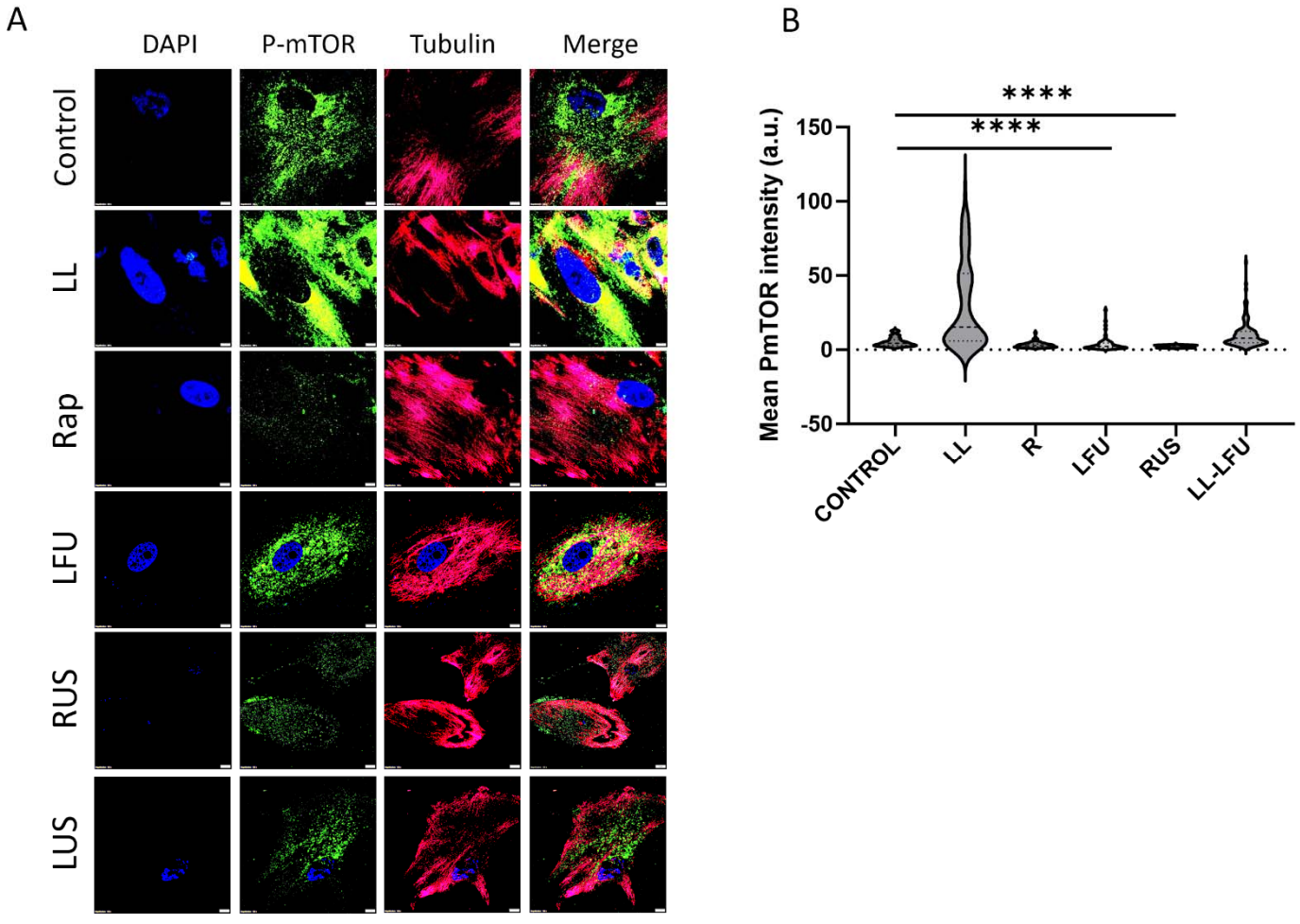

Figure S6: LFU Treatment Causes a Decrease in mTORC1 Activity Synergistic with Rapamycin.
(A), Representative immunofluorescence images of P16 HFF cells (control), (LL) treated L-Leucine (100 mM), (Rap) treated with Rapamycin (1 μM), (LFU) with LFU, (RUS) treated with Rapamycin and LFU, (LUS) treated with LFU and L-Leucine.. Cells were co-immunostained with P-mTORC1 antibody (Green), and Tubulin antibody

(Red), and DAPI (Blue). Scale bar= 10 um. (B), violin plots show the quantification of mean intensity of P-mTORC1 (Green) fluorescence. Result is plotted as mean± s.d. per cell, minimum 15 cells were analyzed. **** p

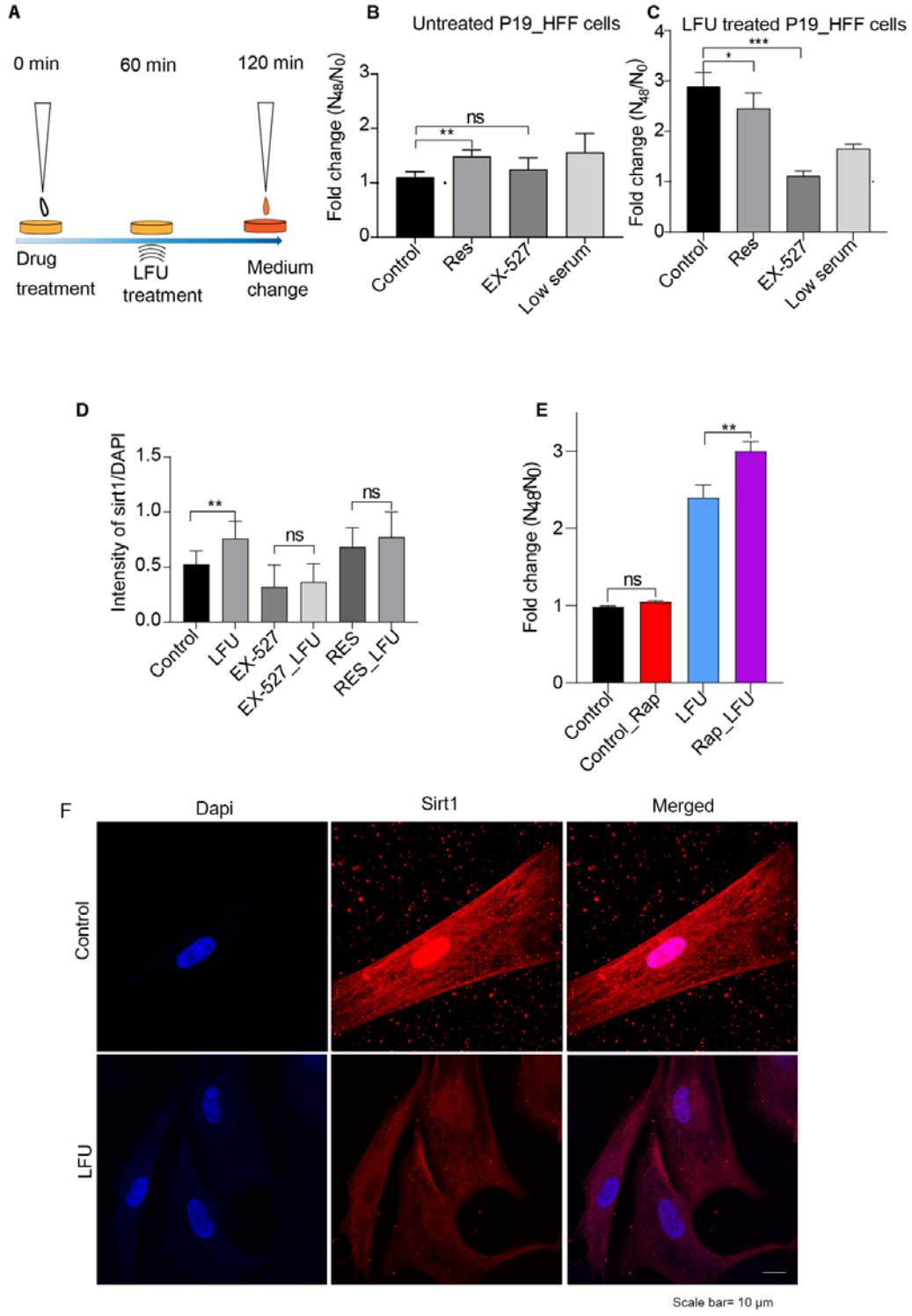

value<0.0001 Two tailed Mann Whitney test was used.

G

Figure S7: Ultrasound has no effect on growth after sirtuin1 inhibition and LFU causes Sirt1 movement to cytoplasm. (A) Schematic of Resveratrol and EX-527 treatment, followed by Ultrasound treatment and medium change. (B) Growth after 48 h of untreated control senescent P19_HFF cells in presence of drugs, and (C) growth after 48 h of LFU treated P19_HFF cells in the presence of the same drugs. (D. quantification of Sirtuin 1 expression by intensity ratio of Sirtuin 1 antibody fluorescence to DAPI fluorescence after no treatment (Control), LFU treatment for 30' (LFU), 10 μM of EX-527 treatment (EX-527), EX-527 and LFU treatment (EX-527_LFU), Resveratrol treatment (RES), and Resveratrol plus LFU treatment. (E) Growth rate after 48 h of P19 HFF (Control),

treated with Rapamycin (1 μM) (Control_RAP), treated with LFU (LFU) or treated with Rapamycin plus LFU (RAP_LFU) shows significantly increased growth with rapamycin and LFU treated SCs compared to with and without rapamycin controls. (F) Images of DAPI and Sirt1 antibody stained senescent cells before and after LFU treatment. Results are shown as mean ± SD, *P<0.05, **P<0.002, *** P<0.0001.

Figure S8: DNA methylation levels and Telomere Lengths are restored to normal levels after LFU treatment. (A) Fluorescence images of passage 2 (P2), untreated P18 (P18_C) and LFU treated P18 cells (P18_LFU) HFF cells with BrdU and 5 mc fluorescence. (B) Quantification of intensity of 5mc fluorescence. (C) Telomere length measurements of HFFs after passage 2 (P2) and passage 22 (P22) C) shows shortening but length increases

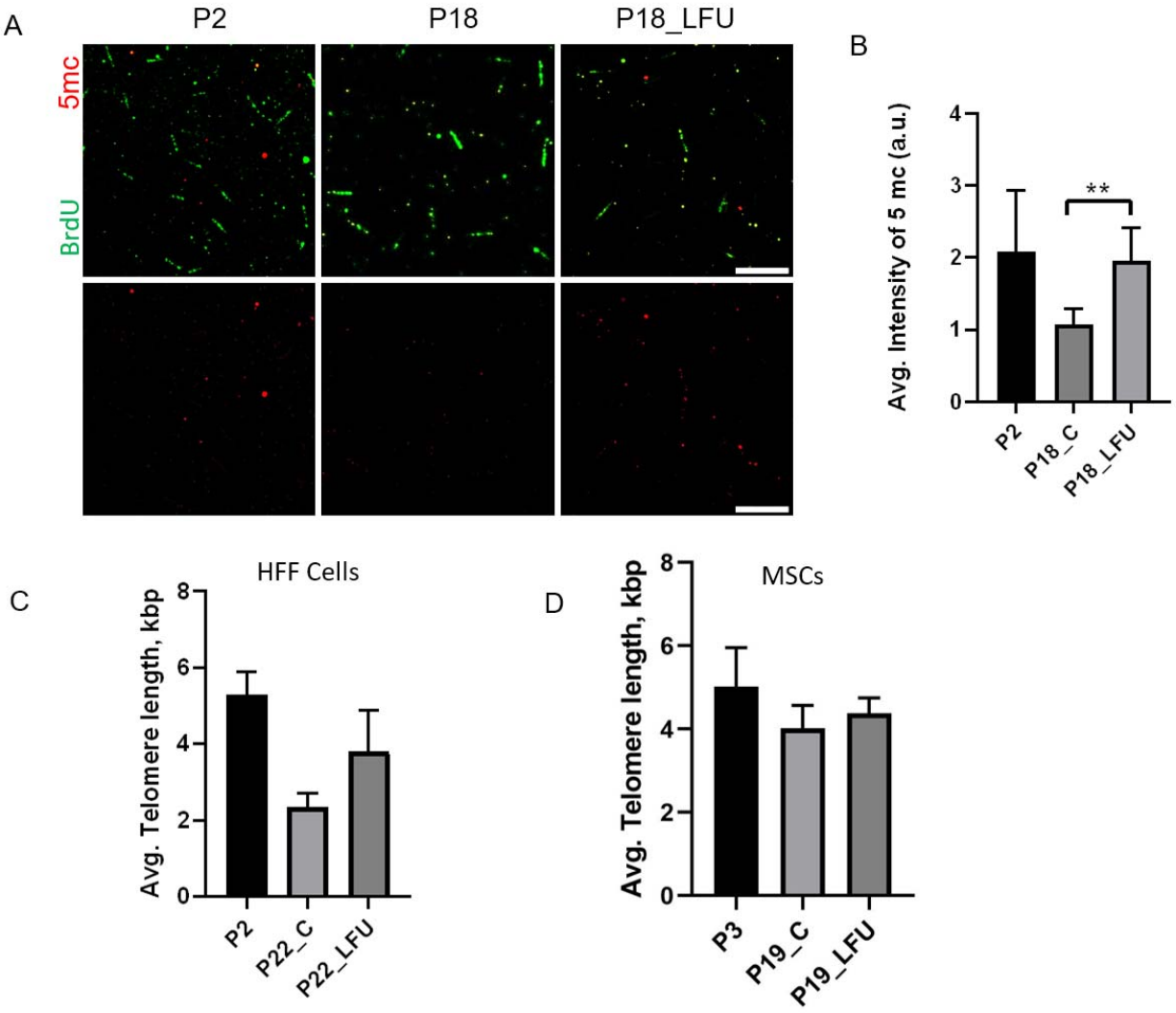

with LFU (P22_LFU) n=4, N=1. Results are shown as mean ± SD. (D) In mesenchymal stem cells, the telomere length decreases slightly from passage 3 (P3) to passage 19 (P19_C) but is increased proportionally by LFU (P19_LFU), n=6 from one experiment. Results are shown as mean ± SD from the three independent experiments. Scale bar= 10 μm, *** P<0.0001.

Figure S9 Rejuvenation of senescent cells involve TRPV1 and Piezi1 activation. (A) Representative Immunofluorescence-stained images of 3 day old bleomycin-sulfate-induced senescent cells. Cells were treated with

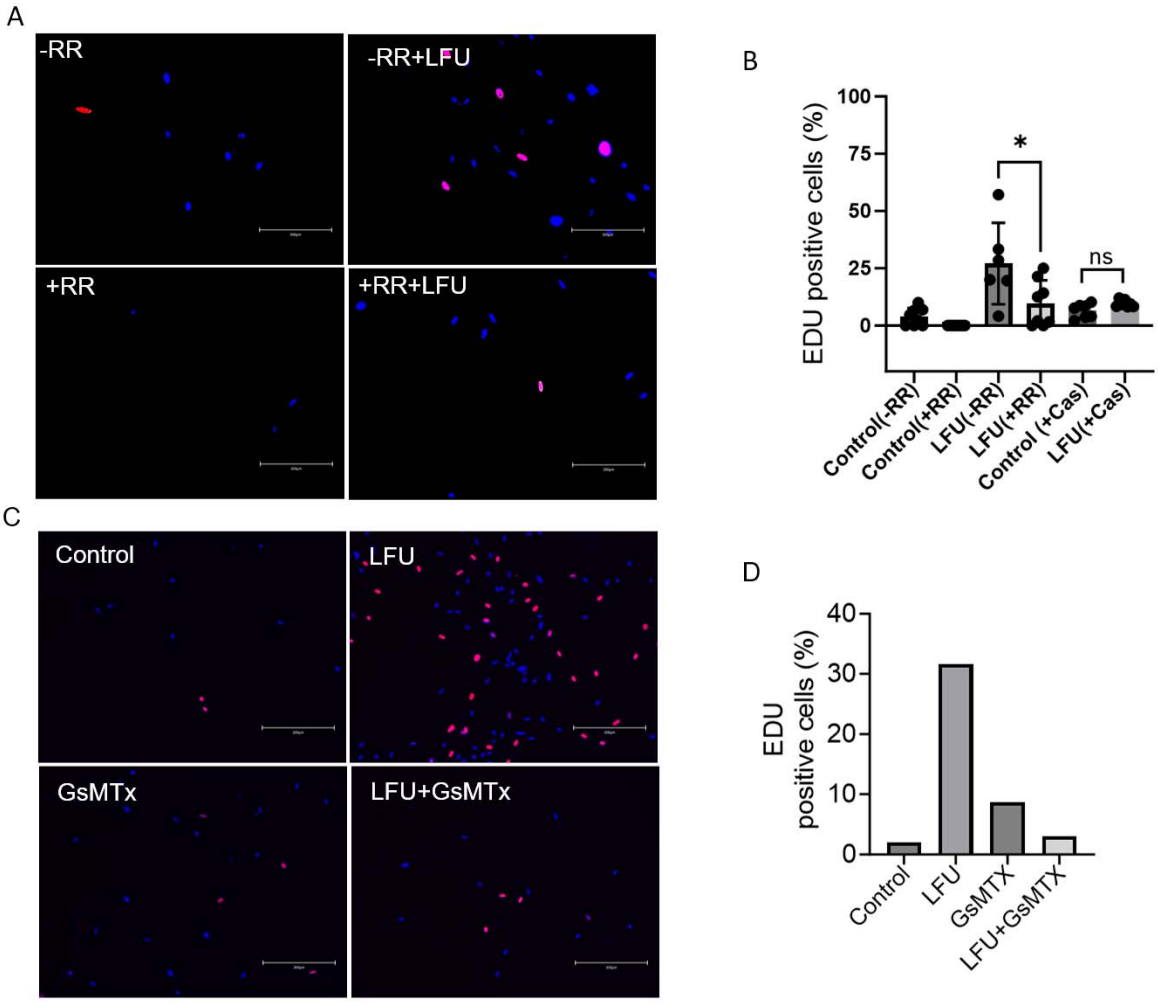

1310 or without LFU in presence or absence of TRPV1 inhibitor, Ruthenium Red (RR). Caspaicin (Cas) was used to activate TRPV1(Images are not shown). Scale bar= 300 µm. Cells were then incubated for 12 h in EDU reagents and stained for EDU (red staining) as well as nuclei (DAPI stained, blue). (B), quantification of proliferating cells by manually 1315 counting the red colored nuclei. EDU positive cells, and dividing by the total number of cells in the fields. Results are plotted as the mean of three independent experiments ± s.d. * p value < 0.05 using unpaired two tailed test, more than 100 cells were counted in each condition. (C) Representative immunofluorescence images of Bleomycin sulphate treated Human foreskin fibroblast (HFF) treated with or without LFU in presence or absence of piezo1 1320 inhibitor, GsMTx and control (untreated) cells stained for nuclei (DAPI stained, blue) and EDU positive cells- red). Scale bar= 300 µm. Experiment was performed once.